Electronic Supplementary Material (ESI) for Physical Chemistry Chemical Physics.

Electronic Supplementary Information

A comprehensive picture of the ultrafast excited-state dynamics of retinal

Oliver Flender, Mirko Scholz, Jonas Hölzer,

Kawon Oum and Thomas Lenzer**

Universität Siegen, Physikalische Chemie, Adolf-Reichwein-Str. 2, 57076 Siegen, Germany,
E-mail: oum@chemie.uni-siegen.de, lenzer@chemie.uni-siegen.de

Table of Contents

Chemical structures

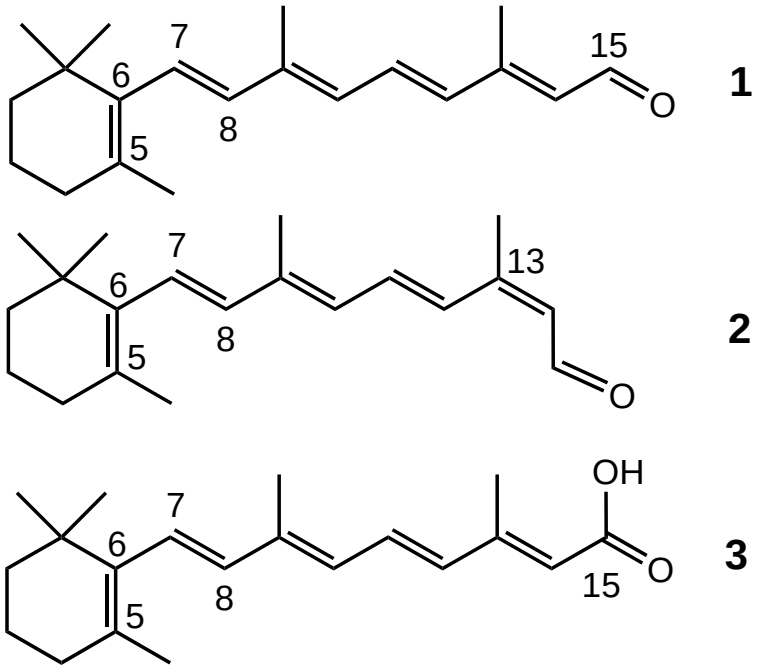

Fig. S1 Chemical structures of all-*trans* retinal (1), 13-*cis* retinal (2), and all-*trans* retinoic acid (3).

Pump fluence dependence for transient absorption signals of all-*trans* retinal in *n*-hexane and acetonitrile

The dependence of the PSCP signals on pump pulse fluence was investigated in separate experiments in the solvents *n*-hexane and acetonitrile. The fluence F_{pump} of the 400 nm pump pulse was varied between 0 and 0.76 mJ cm^{-2} by using pellicle beam splitters. As expected, the amplitudes of the PSCP spectra increased with higher fluence. Results are shown in Figs. S2-S7. These are shown on two different time scales, for instance in the case of *n*-hexane, at 0.17 ps (S_1 and ICT) near 513 nm and those of the GSB at 361 nm (Fig. S2). Data for longer time scales are shown for the T_1 triplet state at 444 nm (Fig. S3). Figure S4 compares time traces of the T_1 dynamics at 444 nm at four different fluences. As demonstrated in the insets of Figs. S2 and S3, the signal amplitude is linearly dependent on the fluence up to *ca.* 0.3 mJ cm^{-2}, and only levels off slightly at higher fluences. The PSCP experiments in the main manuscript were therefore carried out in the linear regime at a pump pulse fluence of 0.23 mJ cm^{-2}.

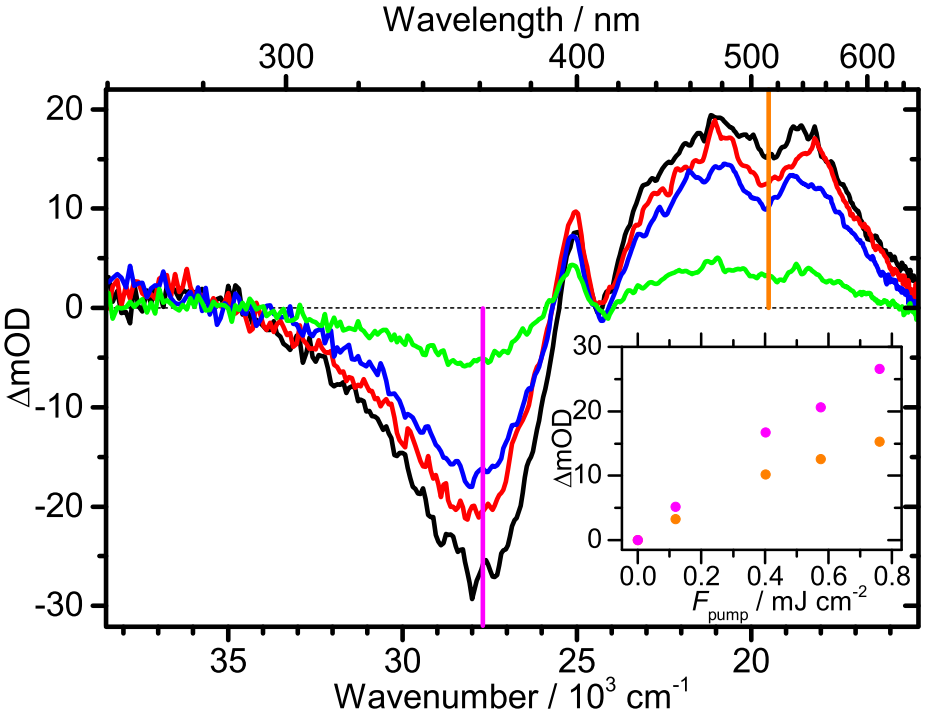

Fig. S2 PSCP spectra of all-*trans* retinal in *n*-hexane at 0.17 ps for different fluences of the 400 nm pump pulse: 0.76 (black), 0.58 (red), 0.40 (blue) and 0.12 mJ cm^{-2} (green). Inset: Amplitudes of each transient signal at 19500 cm^{-1} (orange solid line) and 27700 cm^{-1} scaled by a factor of -1 (magenta solid line) are plotted as a function of the pump pulse fluence.

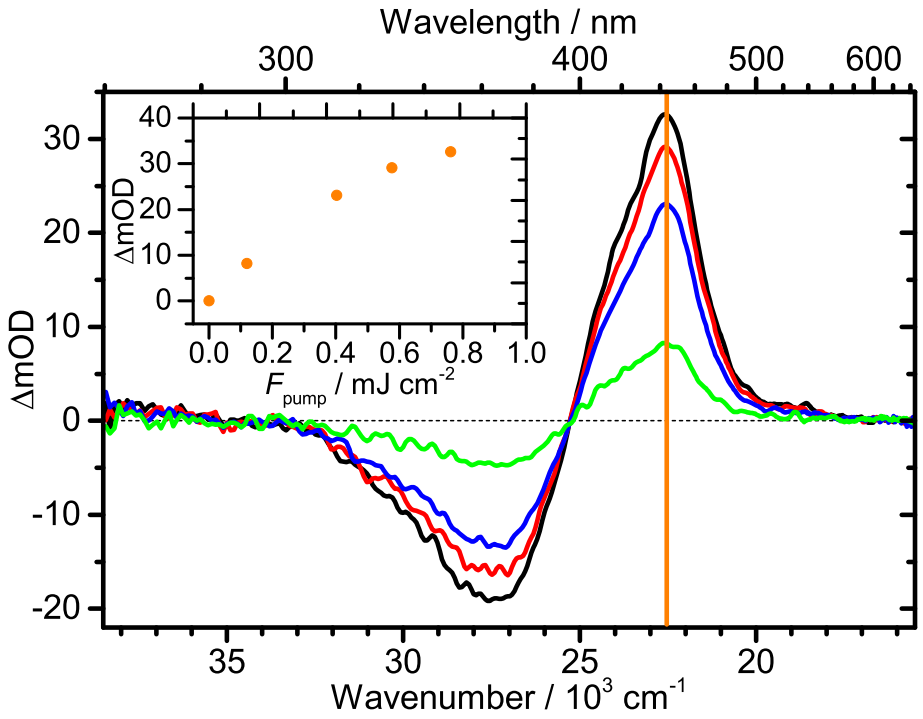

Fig. S3 PSCP spectra of all-*trans* retinal in *n*-hexane at 400 ps for different fluences of the pump pulse at 400 nm: 0.76 (black), 0.58 (red), 0.40 (blue) and 0.12 mJ cm^{-2} (green). The amplitudes at 22500 cm^{-1} (orange solid line) were averaged over the time range 250-497 ps and then plotted as a function of the pump pulse fluence in the inset.

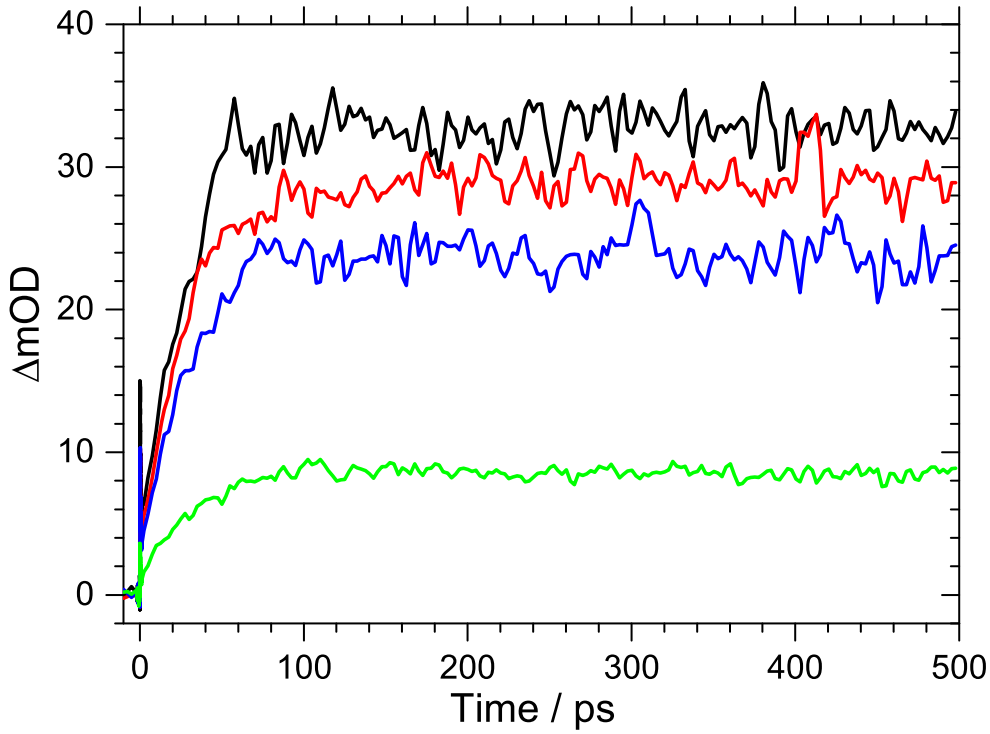

Fig. S4 Kinetics of the T_1 state on longer time scales for all-*trans* retinal in *n*-hexane. Kinetics at different fluences are shown, compare the corresponding PSCP spectra in Fig. S3: 0.76 (black), 0.58 (red), 0.40 (blue) and 0.12 mJ cm^{-2} (green).

For the experiments in acetonitrile, the fluence of the pump pulse at 400 nm was varied in the range of 0-0.92 mJ cm^{-2} by using pellicle beam splitters. They are shown on two different time scales, for instance, at 0.17 ps for the spectral features of the S_1 and ICT species near 19150 cm^{-1} and for those of the GSB near 26500 cm^{-1} (Fig. S5), and on longer time scales for the triplet state (T_1) near 22500 cm^{-1} (Fig. S6). In Fig. S7, we further compare time traces of the T_1 dynamics at 22500 cm^{-1} at four different fluences. Similar to the experiments in *n*-hexane, the amplitude of the PSCP signal increases linearly with pump fluence up to *ca.* 0.3 mJ cm^{-2} but slowly levels off at higher fluences, as can be seen in the insets of both figures. We note that the amplitudes in the inset of Fig. S6 are averaged over the time range 250-497 ps, because the T_1 signal in this time range is essentially constant due to the long lifetime of the triplet state. The PSCP experiments reported in the main manuscript were therefore carried out in the linear regime at a pump pulse fluence of 0.23 mJ cm^{-2}. At a fluence of 0.92 mJ cm^{-2} another maximum appears in the ESA band at around 17000 cm^{-1} which is still visible as a shoulder at fluences of 0.70 and 0.54 mJ cm^{-2}. It is highly likely that the retinal radical cation is formed at these fluences due to 2-photon ionization, compare our previous studies of β-apo-12'-carotenoic acid.[1] The retinal radical cation has a sufficiently long lifetime to appear in the PSCP spectra on long time scales and shows absorption at this energy.[2]

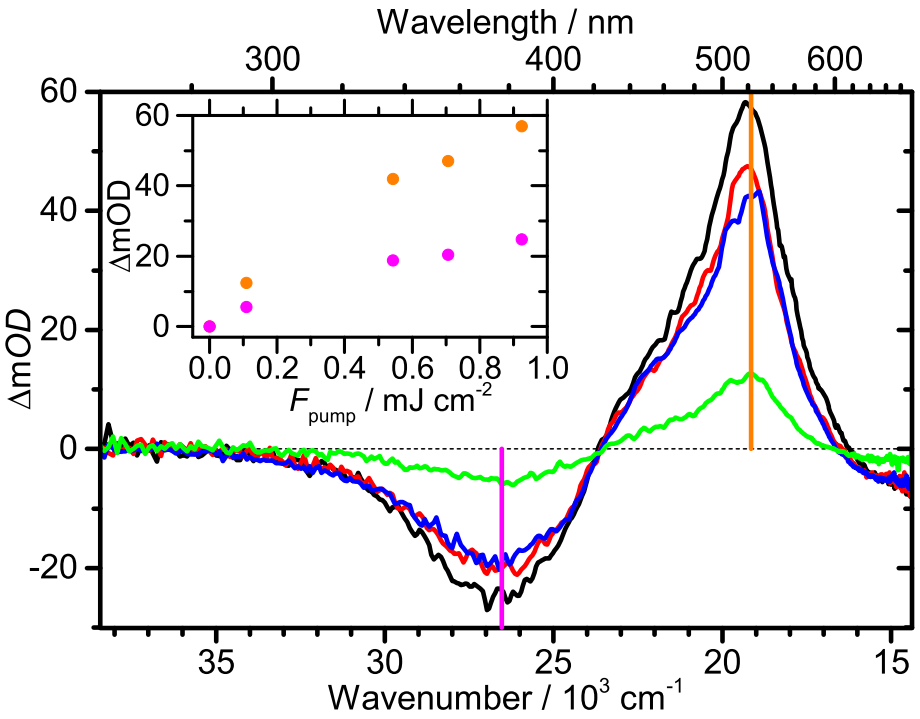

Fig. S5 PSCP spectra of all-*trans* retinal in acetonitrile at 0.17 ps for different fluences of the pump pulse at 400 nm: 0.92 (black), 0.70 (red), 0.54 (blue) and 0.11 mJ cm^{-2} (green). Inset: The amplitudes of each transient signal at 19150 cm^{-1} (orange solid line) and 26500 cm^{-1} scaled by a factor of -1 (magenta solid line) are plotted as a function of the fluence of the pump pulse.

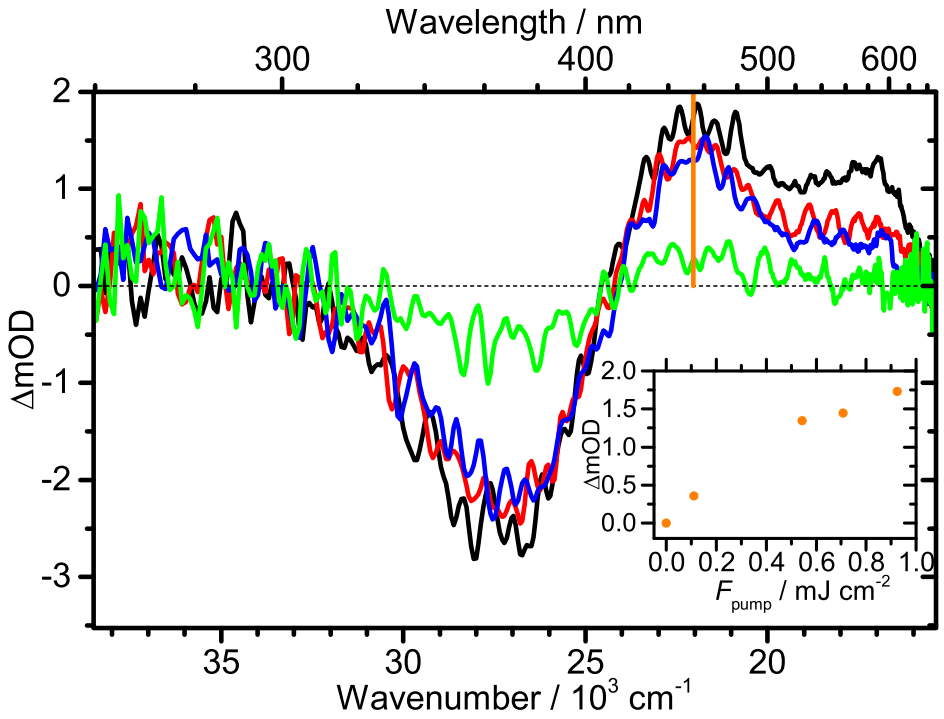

Fig. S6 PSCP spectra of all-*trans* retinal in acetonitrile averaged from 250 to 497 ps at different fluences of the pump pulse at 400 nm: 0.92 (black), 0.70 (red), 0.54 (blue) and 0.11 mJ cm^{-2} (green). The amplitudes at 22045 cm^{-1} (orange solid line) are averaged over the time range 250-497 ps and are plotted in the inset as a function of pump pulse fluence.

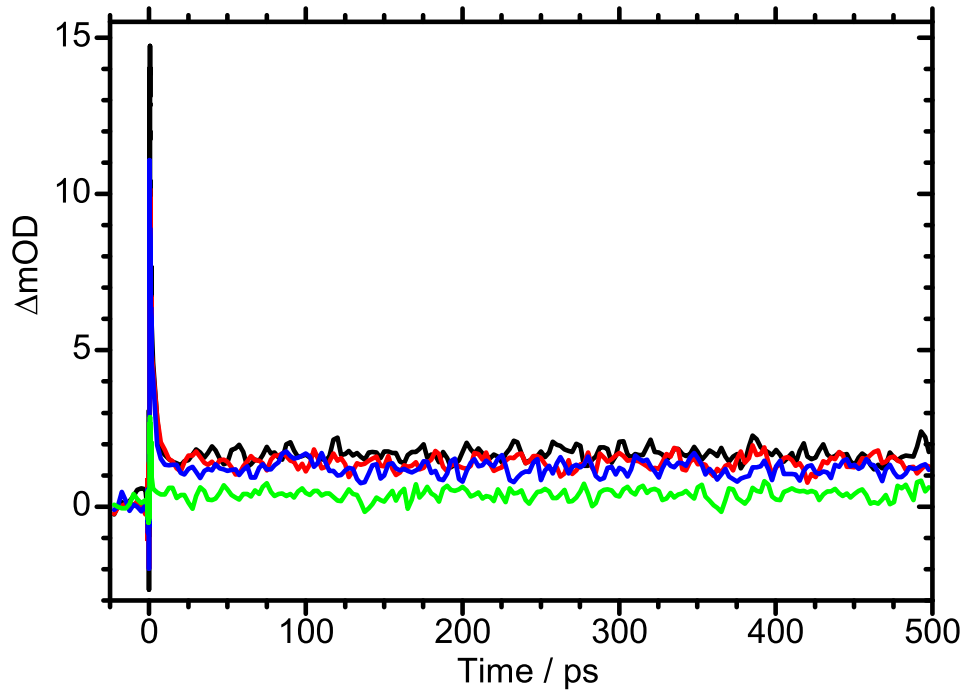

Fig. S7 Kinetics of the T_1 state on longer time scales for all-*trans* retinal in acetonitrile. Kinetics at different fluences are shown, compare the corresponding PSCP spectra in Fig. S5: 0.92 (black), 0.70 (red), 0.54 (blue) and 0.11 mJ cm^{-2} (green).

Subtraction of the solvent contribution in the broadband transient absorption spectra

During the pump-probe overlap time, the broadband transient absorption signals contain considerable nonresonant contributions from the solvent. As discussed previously by Ernsting and co-workers, these include coherent electronic contributions, impulsive stimulated Raman scattering from low-frequency vibrations and Raman signal contributions.[3] Therefore, for all solvents studied, separate solvent spectra were recorded, and these were subtracted from the experiments for retinal and retinoic acid. One example for all-*trans* retinal in the solvent *n*-hexane is shown in Fig. S8. The solvent response in (B) is dominated by sharp positive and negative *anti*-Stokes and Stokes Raman contributions due to the C-H stretching modes of *n*-hexane, symmetrically placed around the center energy of the pump beam. In addition, a broader background of a coherent electronic response is seen which grows toward shorter wavelengths. As shown in (C), the solvent contributions can be completely eliminated by subtraction, (A)-(B), note in particular the flat response in the deep UV region below 300 nm. The remaining structure is due to the coherent response of all-*trans* retinal. We note that for the solvents diisopropyl ether, THF, ethanol and methanol, the solvent contributions reach large values of 40-90 mOD around 300 nm. Therefore the correction in this spectral region is not perfect, but still the residual solvent contributions can be clearly distinguished from the response of retinal based on their characteristic time dependence known from the separate solvent experiments.

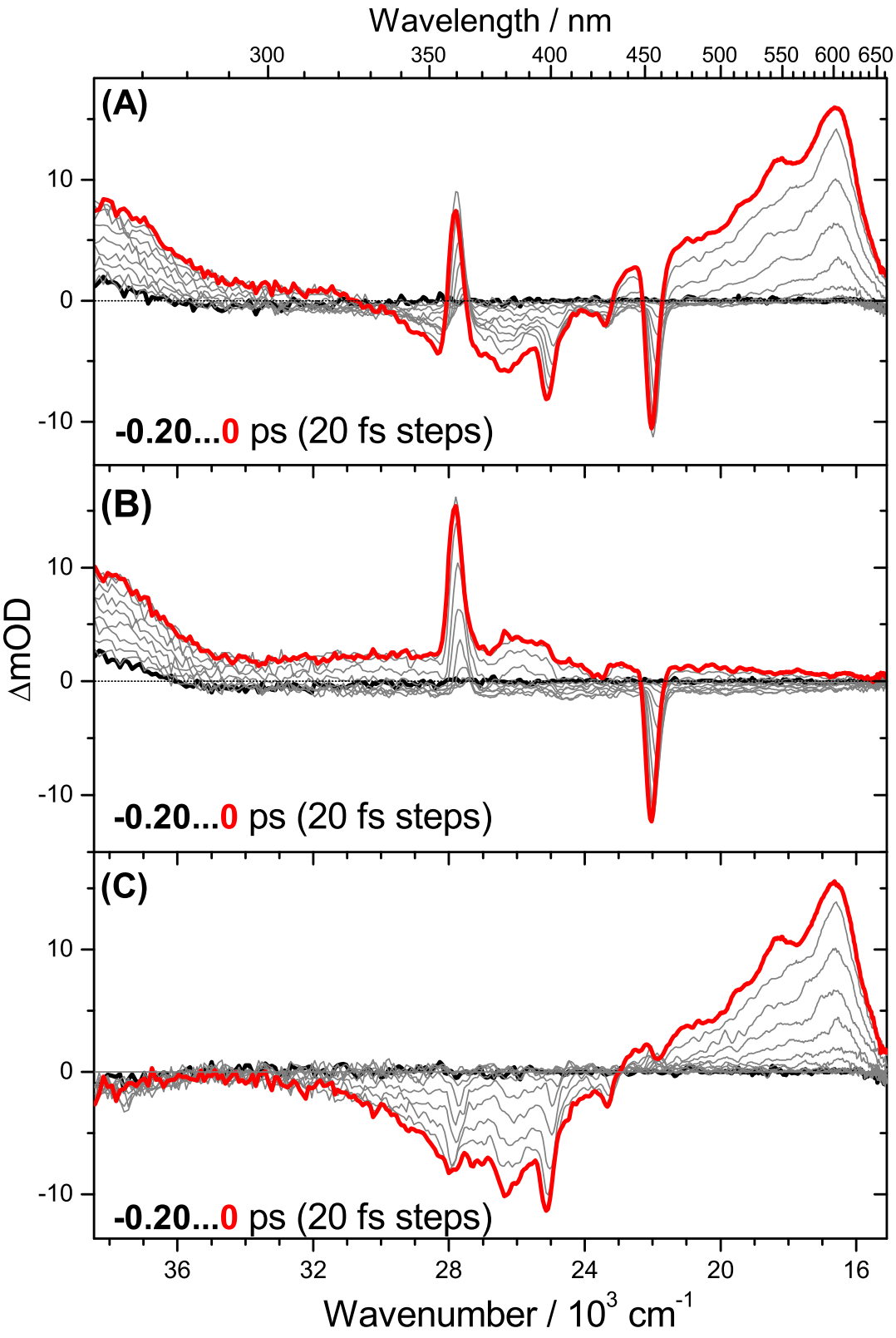

Fig. S8 Subtraction of the solvent contribution in the transient absorption experiments for all-*trans* retinal in *n*-hexane. (A) Raw signal for all-*trans* retinal in *n*-hexane, (B) signal for the pure solvent *n*-hexane, (C) result of the subtraction for the experiments in (A) and (B) providing the pure response of all-*trans* retinal.

Steady-state absorption spectra of all-*trans* and 13-*cis* retinal, their characteristic parameters and solvatochromy analysis

UV-Vis steady-state absorption spectra of the $S_0(^1A_g^-) \rightarrow S_2(^1B_u^+)$ transition of all-*trans* retinal and 13-*cis* retinal in six selected organic solvents at 298 K are shown in Fig. S9. Characteristic parameters, such as the position of the band maximum, absolute absorption coefficients (including error limits from multiple experimental determinations), and the FWHM of the band are summarised in Table S1. The band is unstructured for both isomers, except for a weak shoulder to the blue of the band maximum in alkanes. This is in contrast to longer-chain apocarotenals, where at least in nonpolar solvents partially resolved vibrational progressions are observed.[4,5] The behaviour is consistent with the "distribution of conformers" model of Hemley *et al.*,[6,7] which predicts a stronger influence of the torsional motion of the β-ionone ring on a polyene's effective conjugation length and thus a larger distribution of transition energies leading to a washing-out of vibronic structure. A comparison of all-*trans* and 13-*cis* retinal shows two key differences: For a given solvent, the 13-*cis* spectra are in general slightly blue-shifted and their absolute absorption coefficient reaches on average only 70% of the all-*trans* isomer (Table S1).

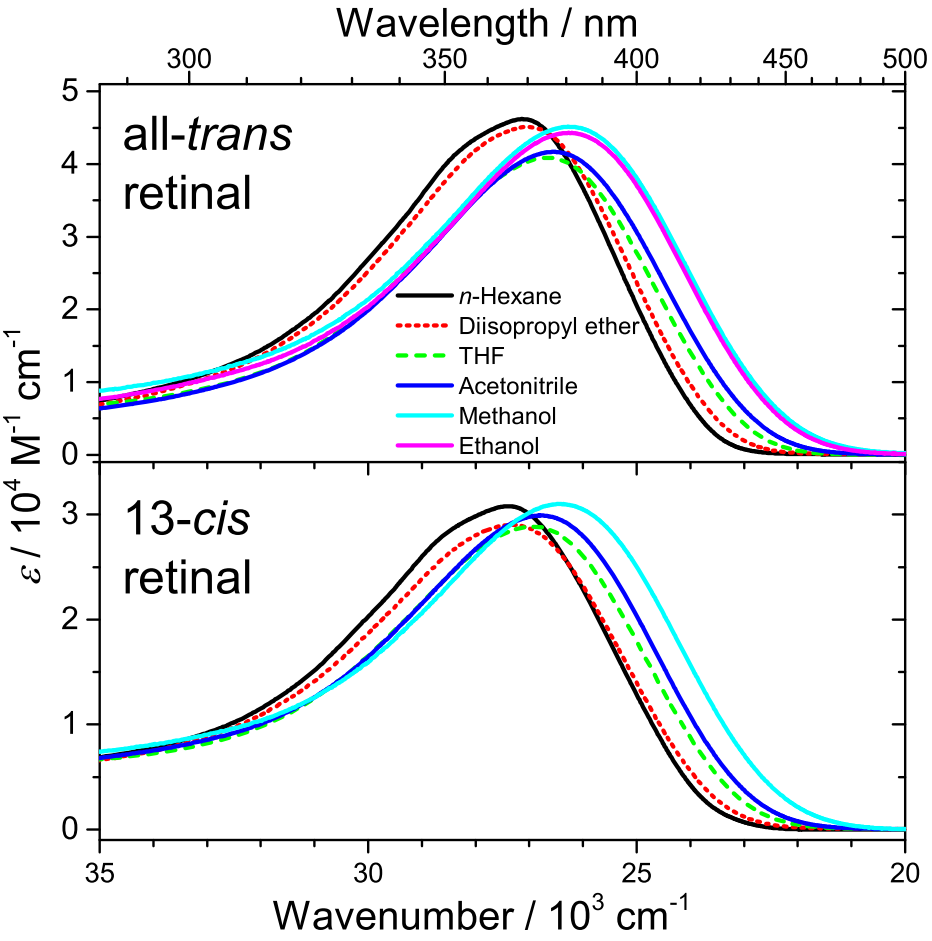

Fig. S9 UV-Vis steady-state absorption spectra of all-*trans* (top) and 13-*cis* retinal (bottom) in the organic solvents *n*-hexane, diisopropyl ether, THF, ethanol, methanol and acetonitrile (298 K).

Table S1 Summary of the room-temperature solvatochromy data for all-*trans* and 13-*cis* retinal in organic solvents including absolute peak absorption coefficients determined for a few key solvents.

Solvent	λ_{max} (nm)		$\tilde{\nu}_{max}$ (cm^{-1})		FWHM (cm^{-1})		ε / 10^4 M^{-1} cm^{-1}	
	all-*trans*	13-*cis*	all-*trans*	13-*cis*	all-*trans*	13-*cis*	all-*trans*	13-*cis*
n-Pentane	368	-	27170	-	5270	-	-	-
n-Hexane	369	365	27090	27400	5260	5690	4.62 ± 0.45	3.08 ± 0.36
i-Octane	369	-	27090	-	5340	-	-	-
n-Hexadecane	373	-	26810	-	5380	-	-	-
Diisopropyl ether	369	366	27090	27320	5460	5840	4.51± 0.12	2.90± 0.16
Ethyl acetate	371	-	26950	-	5570	-	-	-
THF	374	371	26750	26930	5610	5840	4.09± 0.20	2.88± 0.20
n-Butanol	384	-	26040	-	5570	-	-	-
Acetone	374	-	26740	-	5630	-	-	-
Ethanol	379	378	26390	26440	5900	6210	4.43± 0.78	-
Methanol	380	378	26330	26430	6070	6150	4.51 ± 0.32	3.10± 0.86
Acetonitrile	376	374	26600	26790	5680	5860	4.17 ± 0.14	2.99± 0.22

In Fig. S10, we compare steady-state absorption spectra of all-*trans* retinal for all solvents studied, including also *n*-pentane, *i*-octane and *n*-hexadecane. A solvatochromic red-shift of the absorption maxima is clearly visible which is analysed in more detail below.

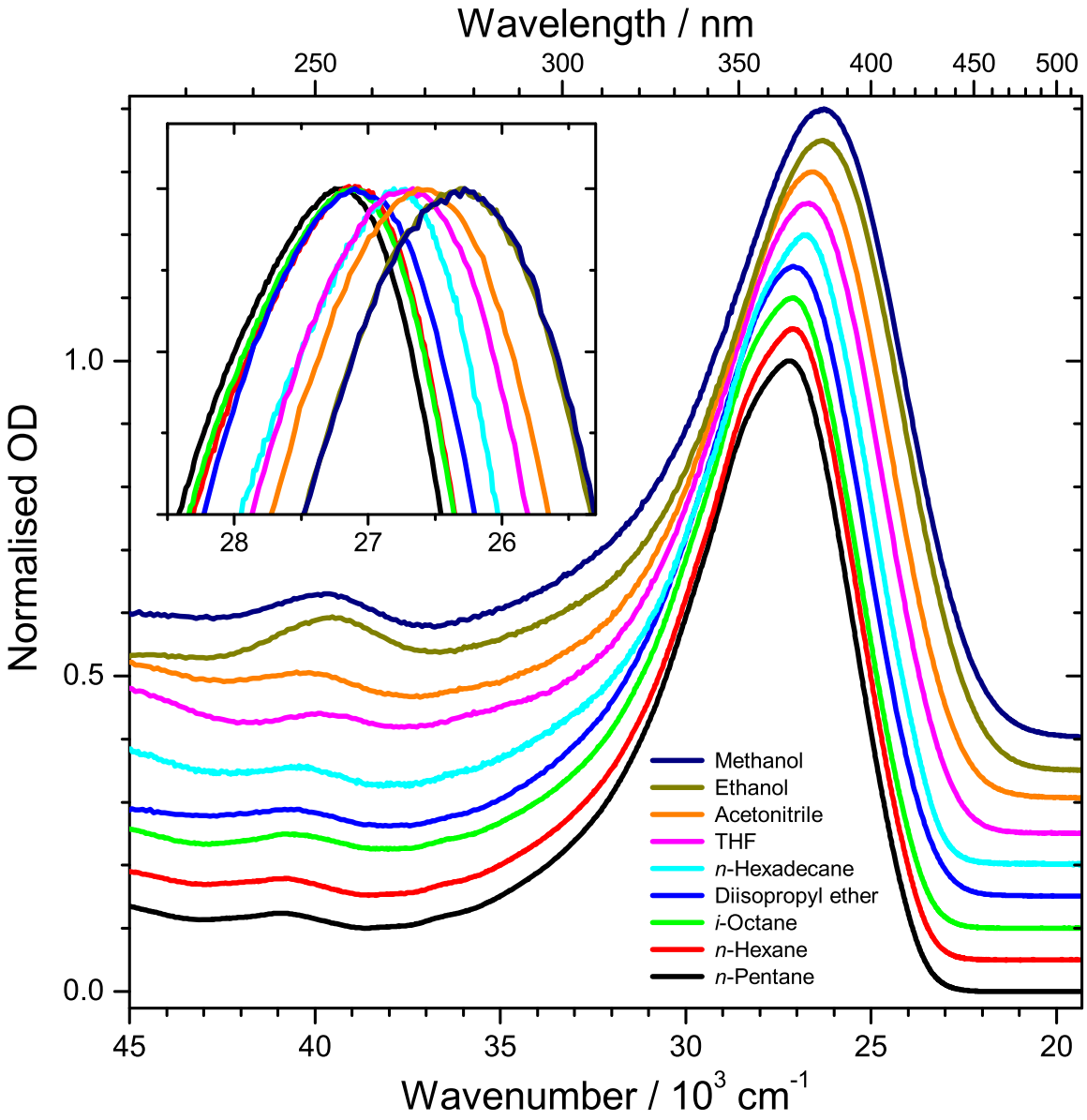

Fig. S10 Normalised steady-state absorption spectra of all-*trans* retinal in various organic solvents. As complementary data to Fig. S9, a comparison for the complete set of solvents is given here, *i.e.* *n*-pentane, *n*-hexane, *i*-octane, *n*-hexadecane, diisopropyl ether, tetrahydrofuran (THF), acetonitrile, ethanol and methanol. The spectra are baseline-shifted to avoid extensive crossings of the spectra. The inset shows a magnification of the peak region.

Figure S11 shows a plot of the maximum of the absorption band *vs.* the Lorenz-Lorentz function $R(n)$, *i.e.* the polarisability of the solvent. The data for the alkanes exhibit an approximately linear dependence (1-4, red circles) suggesting a polarisability-induced spectral red-shift due to a stronger relative stabilisation of S_2 with respect to S_0. The deviations observed for the more polar solvents (5-9, blue squares) indicate that additional solvent properties beyond polarisability affect the band position.

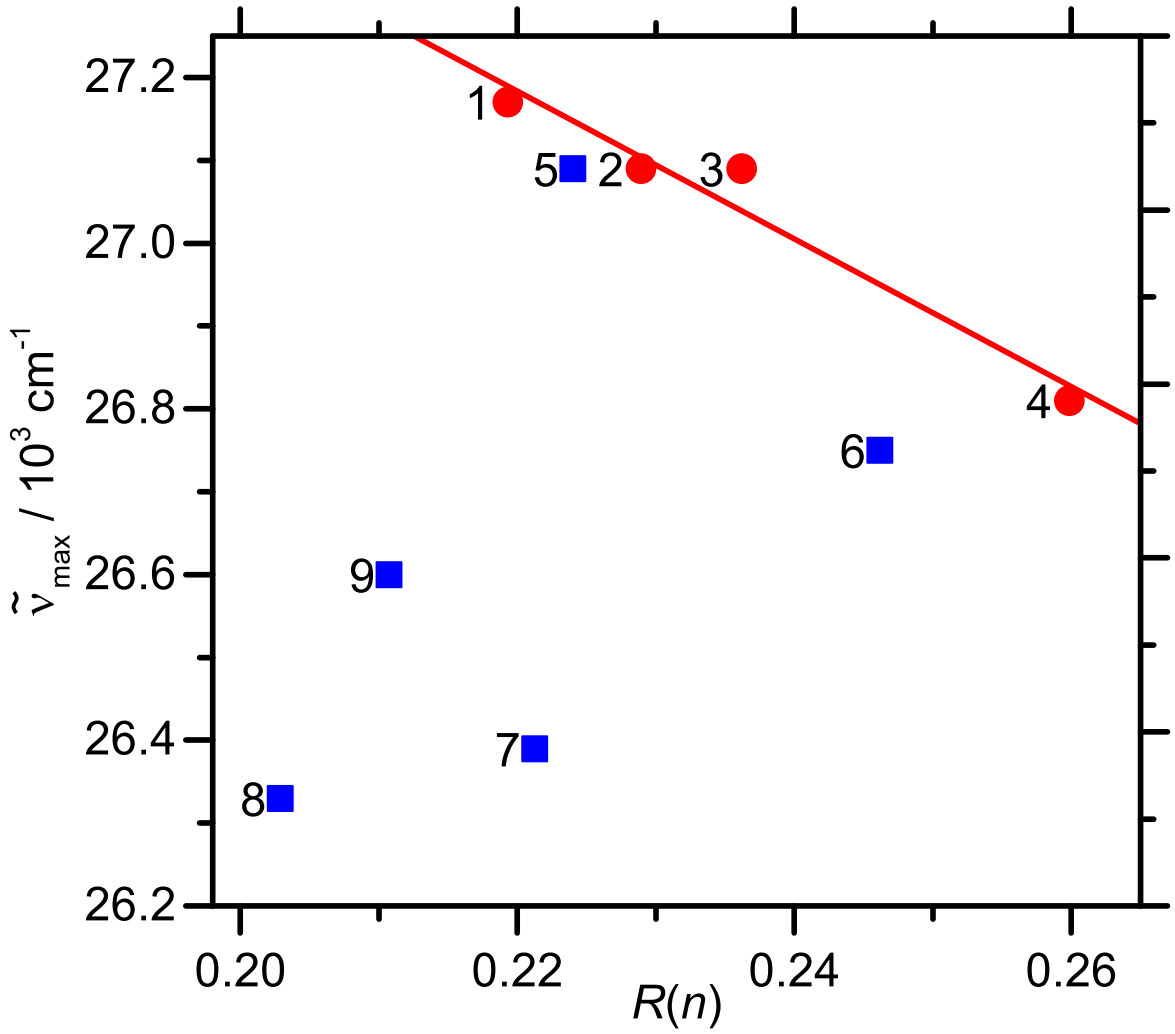

Fig. S11 Position of the maximum of the $S_0 \rightarrow S_2$ absorption band as a function of the polarisability $R(n)$ of the solvent. $R(n) = (n^2-1)/(n^2+2)$, where n is the refractive index of the solvent. (Red circles) 1: *n*-pentane, 2: *n*-hexane, 3: *i*-octane, 4: *n*-hexadecane. (Blue squares) 5: diisopropyl ether, 6: THF, 7: ethanol, 8: methanol, 9: acetonitrile. The red line is the result of a linear fit to the data points of the alkane series.

Figures S12 and S13 show plots using different measures of polarity. In Fig. S12, the maximum of the absorption band is plotted against the electronic and nuclear (dipolar) polarisability of the solvent $R(\varepsilon) = (\varepsilon\text{-}1)/(\varepsilon\text{+}2)$.[8] In Fig. S13 this is done using nuclear solvent polarisability $\Delta f = R(\varepsilon)\text{-}R(n)$ on the abscissa as a measure of dipolarity.[8] While there is a trend of larger red-shift for larger $R(\varepsilon)$ and Δf values, there is no clean correlation. In particular we note the considerably stronger red-shift for ethanol and methanol (7 and 8) compared to acetonitrile (9) which suggests an additional influence of hydrogen-bonding. The latter is also supported by the larger FWHM of the spectra in the two alkanols (Table S1) which could be due to the formation of different types of hydrogen-bonded conformers between all-*trans* retinal and the solvent. It therefore appears that an increase of polarisability, polarity and hydrogen-bonding of the solvent all favour a larger red-shift of the absorption spectra (= reduction of the S_0-S_2 energy gap). This behaviour is similar to that observed by us previously for the longer-conjugated β-apo-12'-carotenal.[4,5]

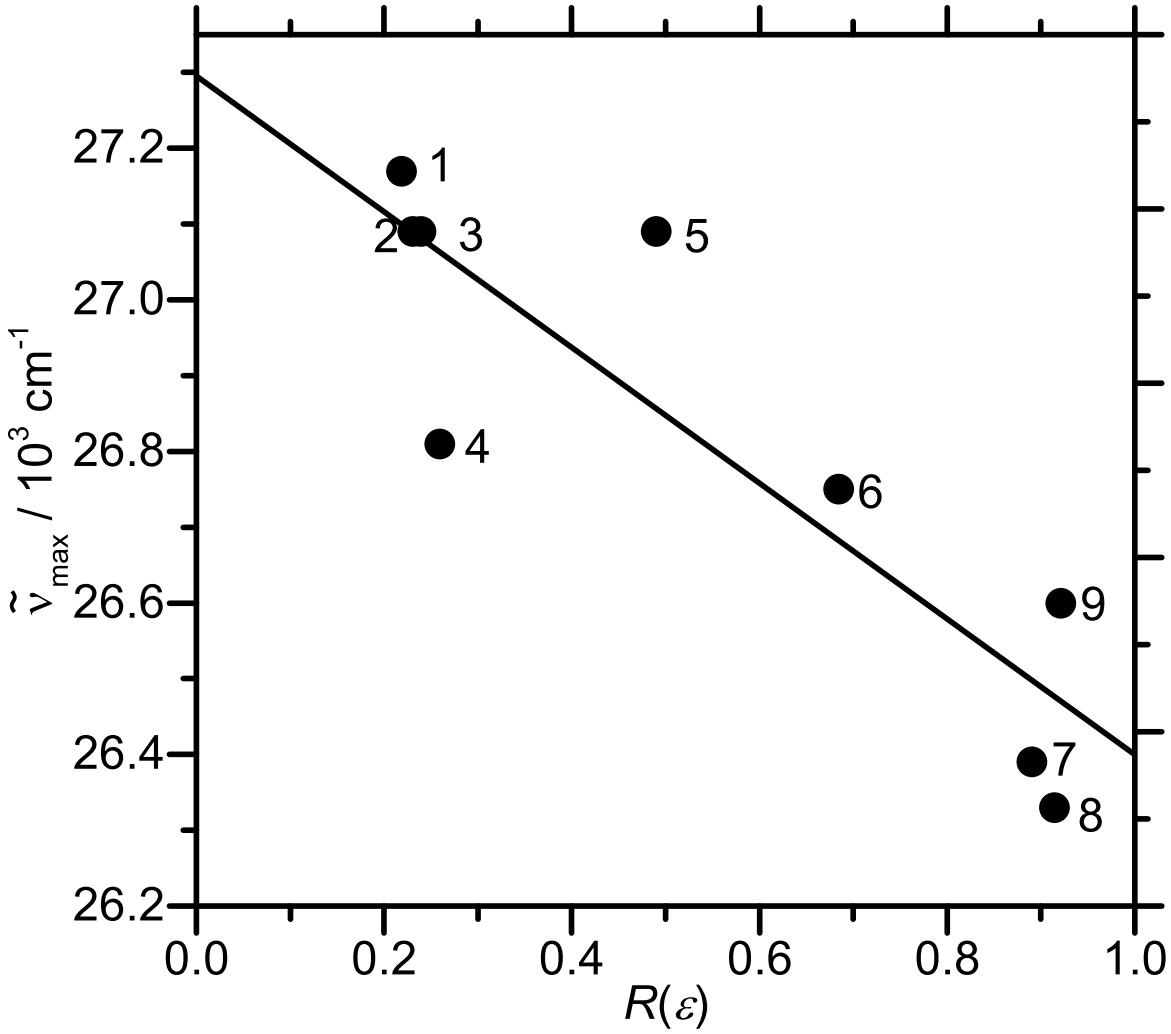

Fig. S12 Position of the maximum of the main absorption band as a function of electronic and nuclear (dipolar) polarisability of the solvent $R(\varepsilon)$. $R(\varepsilon) = (\varepsilon\text{ -}1)/(\varepsilon\text{ +}2)$ where ε is the dielectric constant of the solvent. 1: *n*-pentane, 2: *n*-hexane, 3: *i*-octane, 4: *n*-hexadecane, 5: diisopropyl ether, 6: THF, 7: ethanol, 8: methanol, 9: acetonitrile.

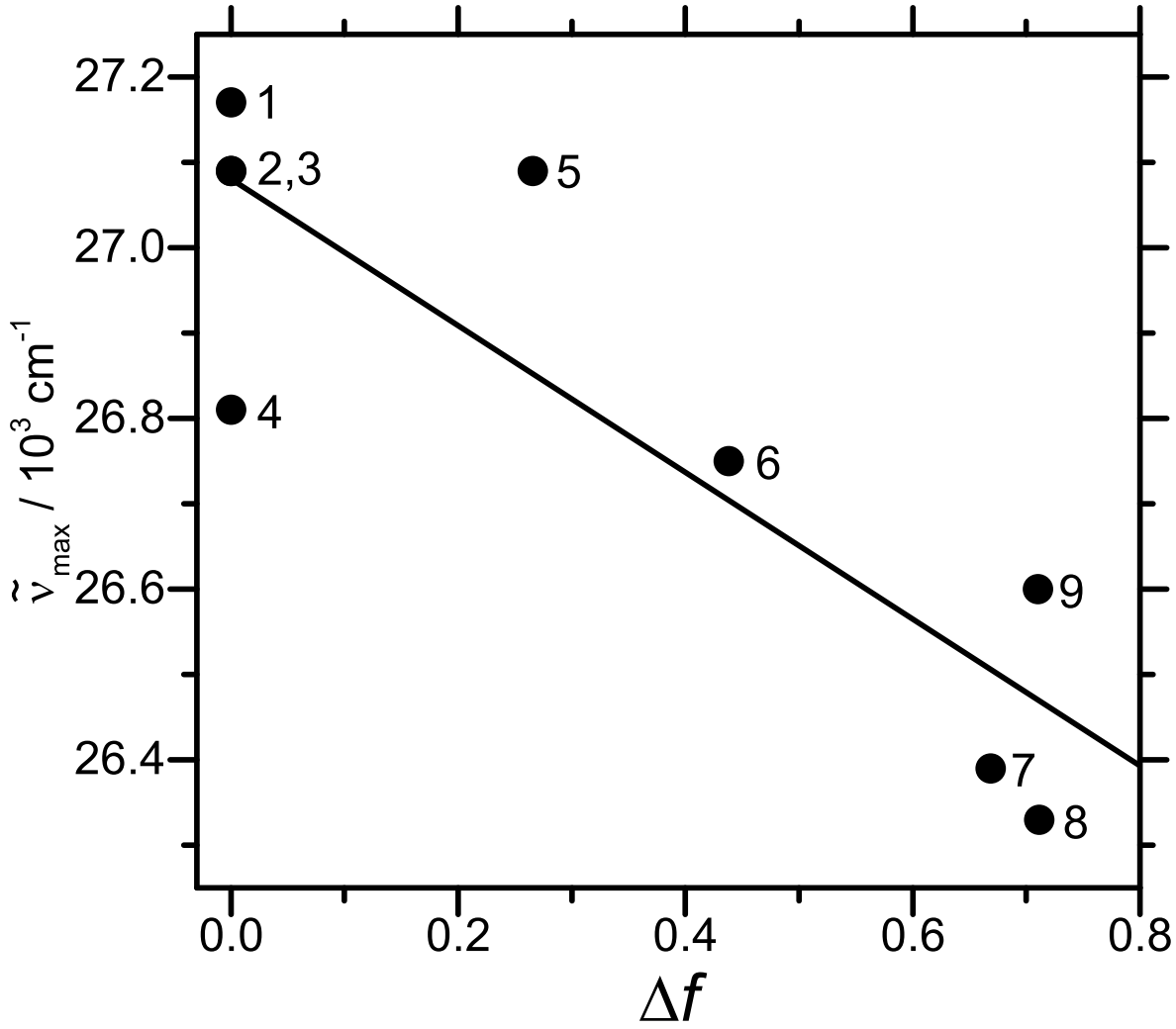

Fig. S13 Position of the maximum of the main absorption band as a function of solvent dipolarity Δf. $\Delta f = R(\varepsilon)\text{-}R(n) = (\varepsilon\text{-}1)/(\varepsilon\text{+}2)\text{-}(n^2\text{-}1)/(n^2\text{+}2)$. 1: *n*-pentane, 2: *n*-hexane, 3: *i*-octane, 4: *n*-hexadecane, 5: diisopropyl ether, 6: THF, 7: ethanol, 8: methanol, 9: acetonitrile.

UV-Vis transient broadband absorption spectra of all-*trans* retinal

In Figs. S14-S19 we summarise the PSCP transient absorption spectra of all-*trans* retinal in different organic solvents. The PSCP spectra for *n*-hexane are included in the main manuscript (Fig. 1(A)). Contour plots for the transient spectra of all-*trans* retinal in *n*-hexane, *n*-hexadecane, diisopropyl ether, THF and methanol are included in Figs. 1(C) and 2 (main manuscript).

i) *n*-Hexadecane

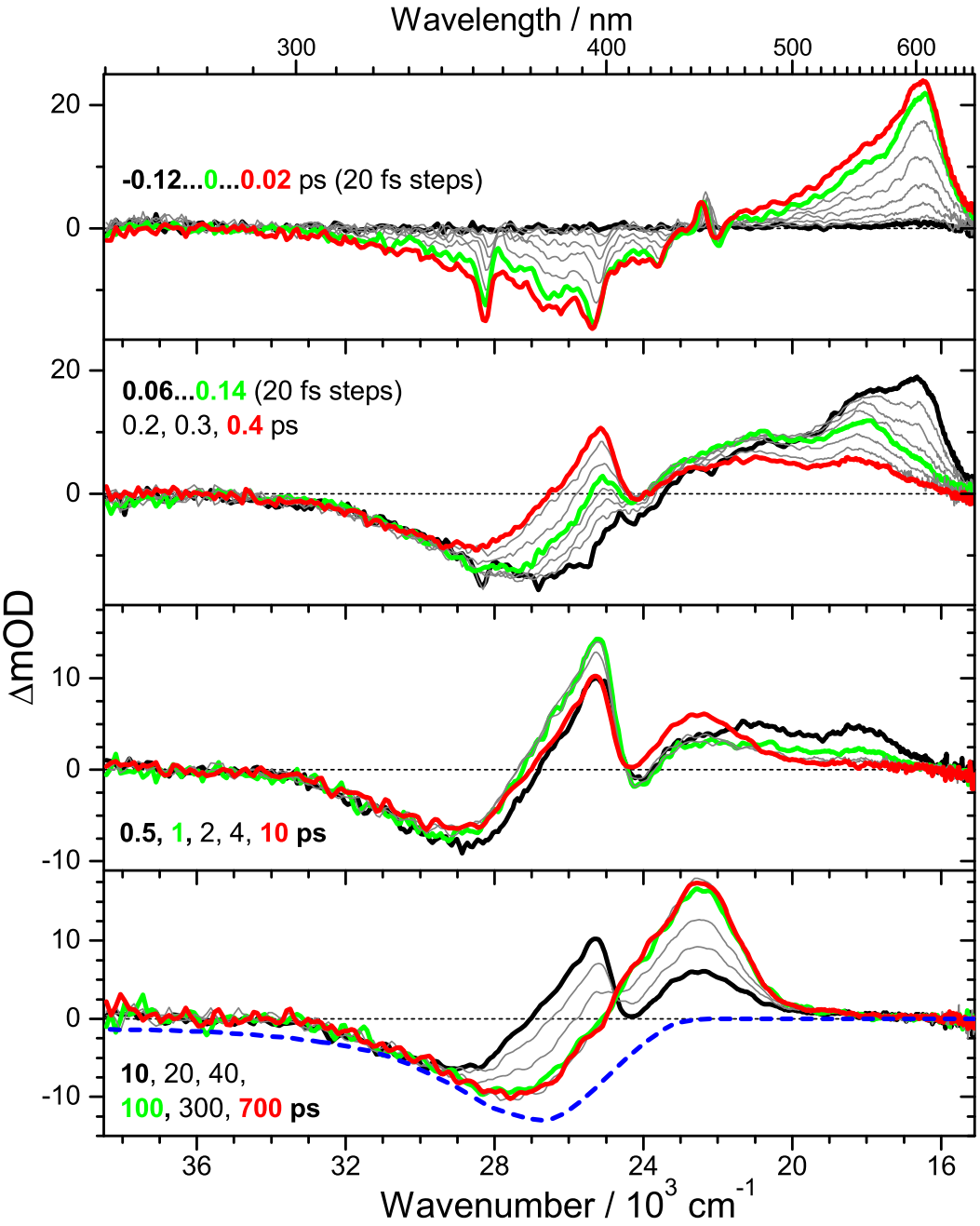

Fig. S14 PSCP transient absorption spectra of all-*trans* retinal in *n*-hexadecane at 298 K. Experimental conditions: λ_{pump} = 400 nm; fluence of the pump pulse *ca.* 0.23 mJ cm^{-2}. In the bottom panel, the inverted steady-state absorption spectrum is shown for comparison.

ii) Diisopropyl ether

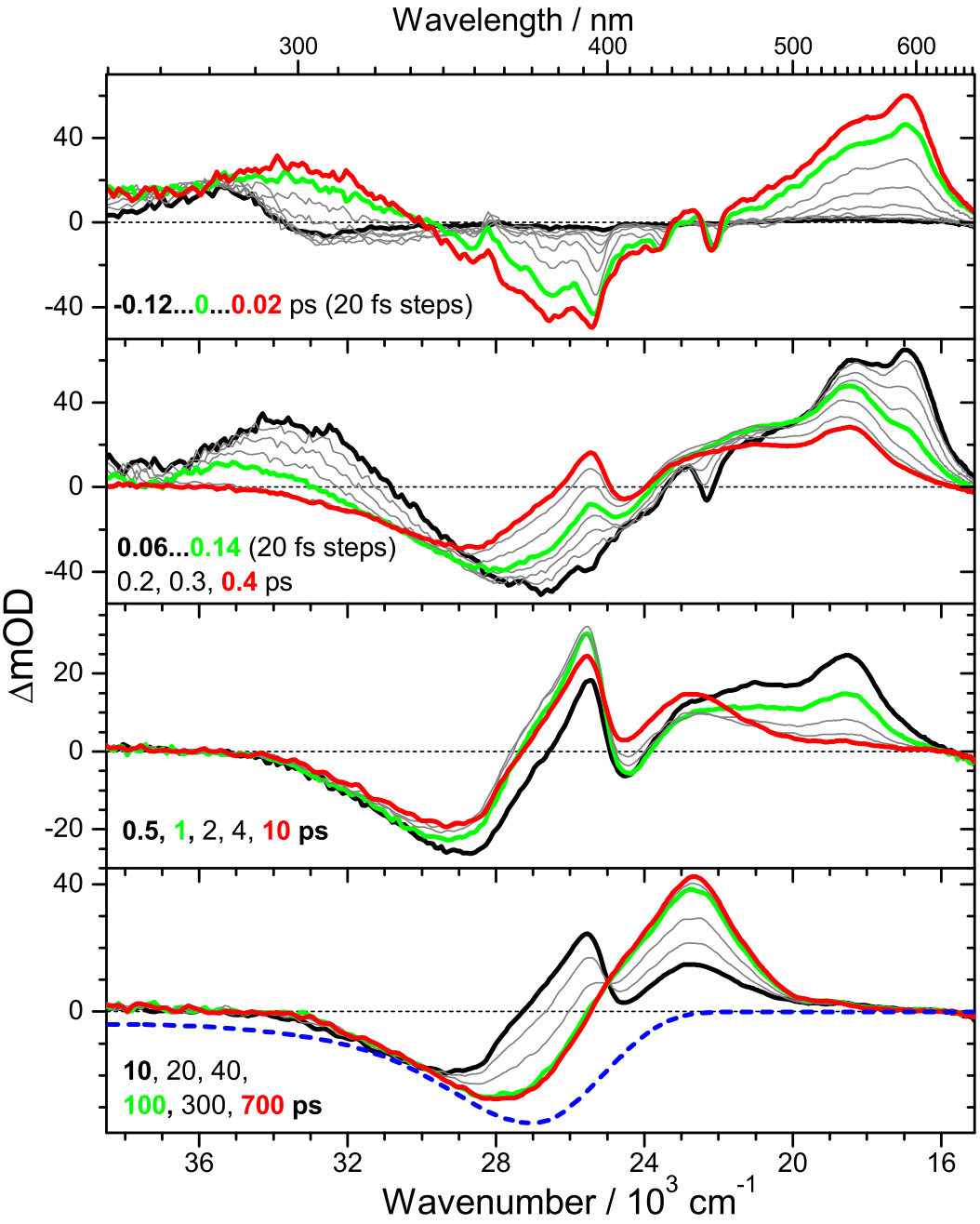

Fig. S15 PSCP transient absorption spectra of all-*trans* retinal in diisopropyl ether at 298 K. Experimental conditions: λ_{pump} = 400 nm; fluence of the pump pulse *ca.* 0.23 mJ cm^{-2}. In the bottom panel, the inverted steady-state absorption spectrum is shown for comparison.

iii) THF

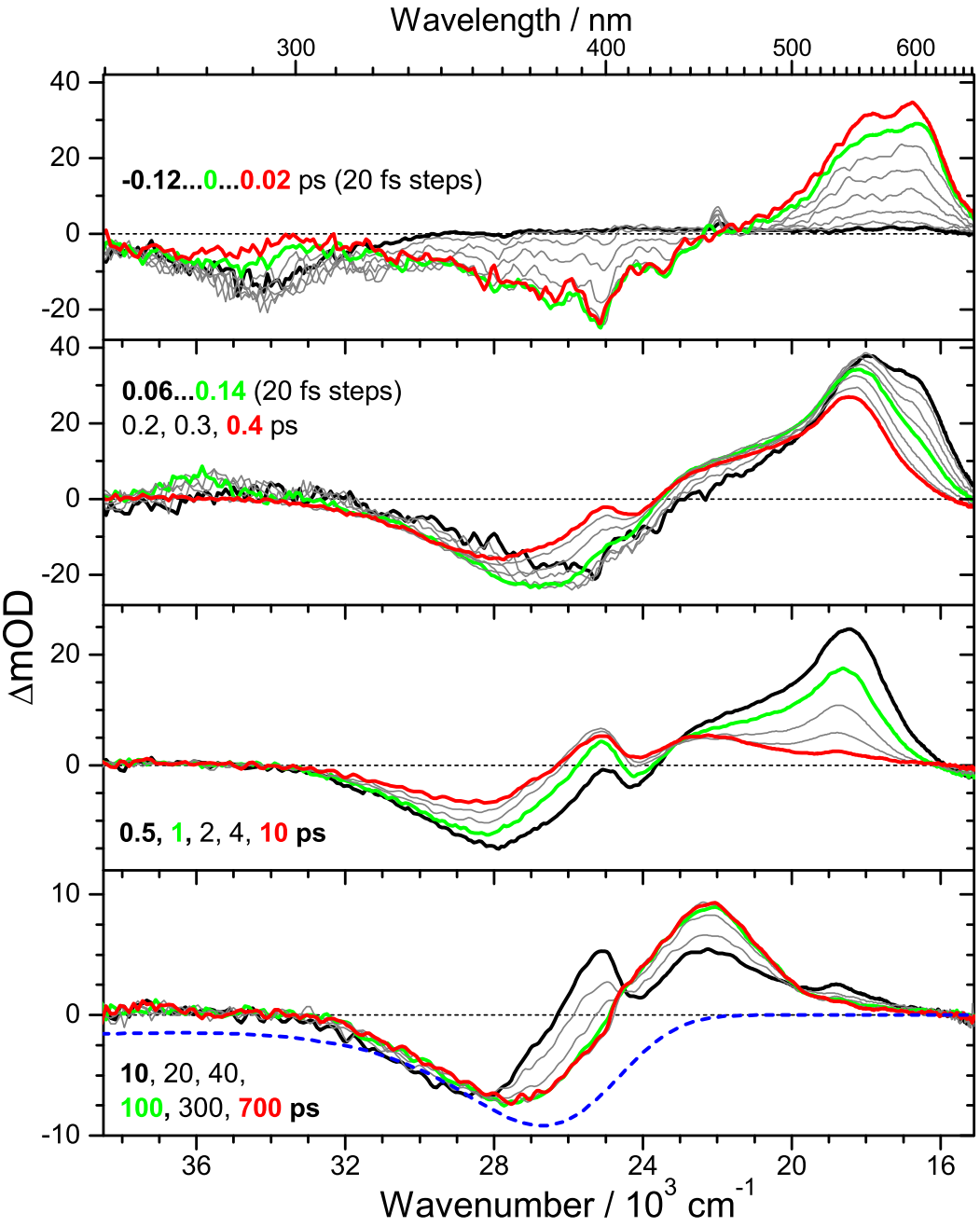

Fig. S16 PSCP transient absorption spectra of all-*trans* retinal in THF at 298 K. Experimental conditions: λ_{pump} = 400 nm; fluence of the pump pulse *ca.* 0.23 mJ cm^{-2}. In the bottom panel, the inverted steady-state absorption spectrum is shown for comparison.

iv) Ethanol

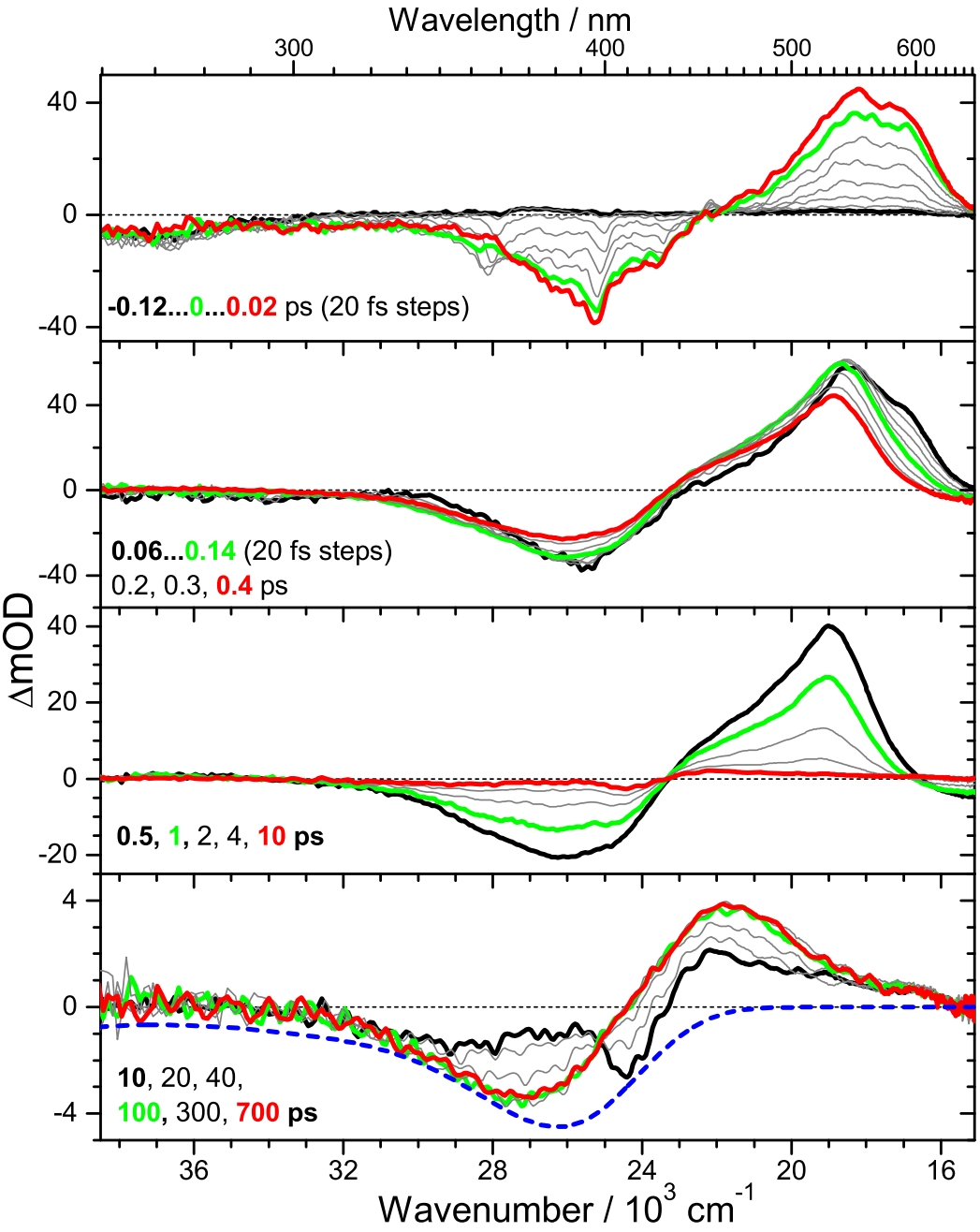

Fig. S17 PSCP transient absorption spectra of all-*trans* retinal in ethanol at 298 K. Experimental conditions: λ_{pump} = 400 nm; fluence of the pump pulse *ca.* 0.23 mJ cm^{-2}. In the bottom panel, the inverted steady-state absorption spectrum is shown for comparison.

v) Methanol

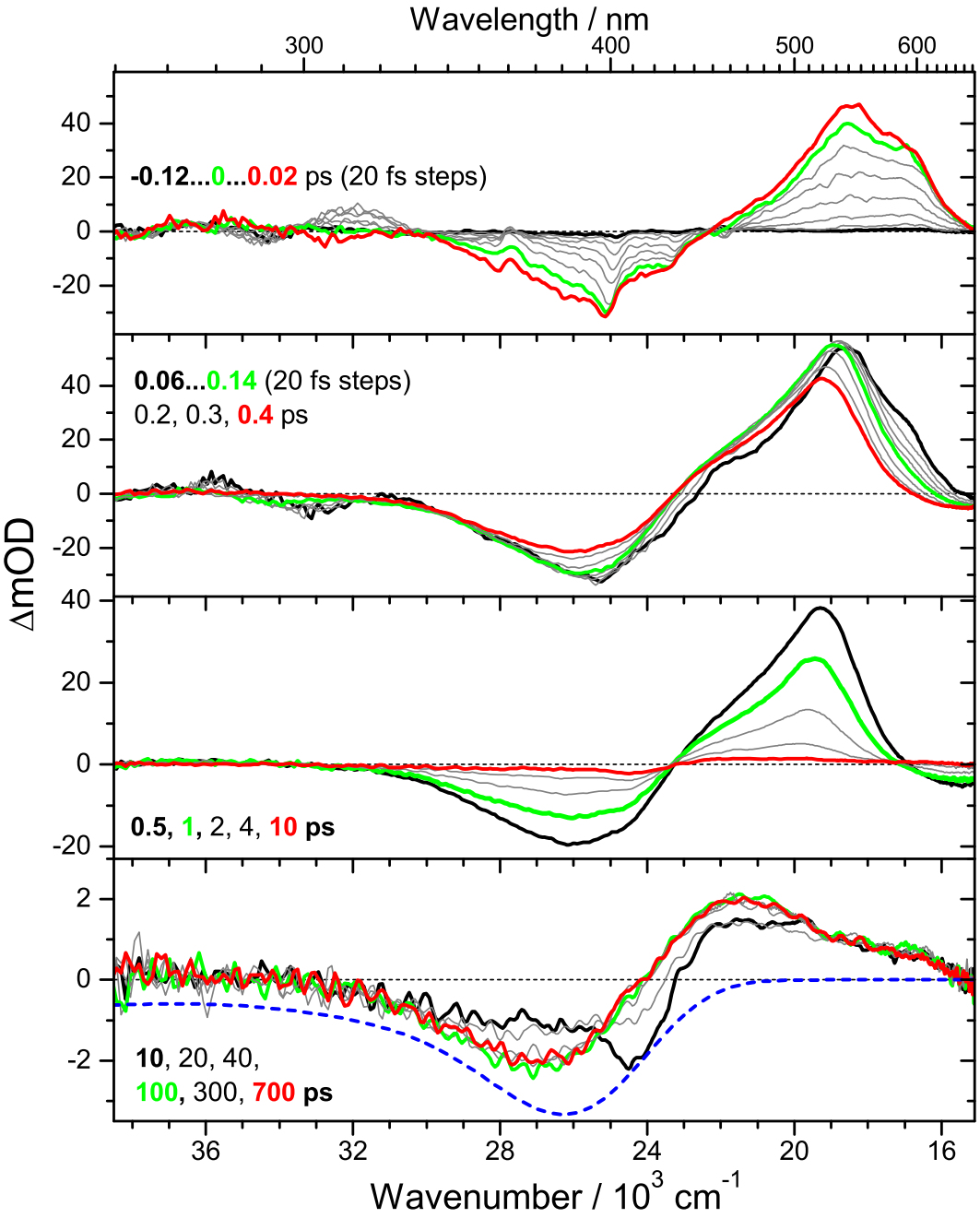

Fig. S18 PSCP transient absorption spectra of all-*trans* retinal in methanol at 298 K. Experimental conditions: λ_{pump} = 400 nm; fluence of the pump pulse *ca.* 0.23 mJ cm^{-2}. In the bottom panel, the inverted steady-state absorption spectrum is shown for comparison.

vi) Acetonitrile

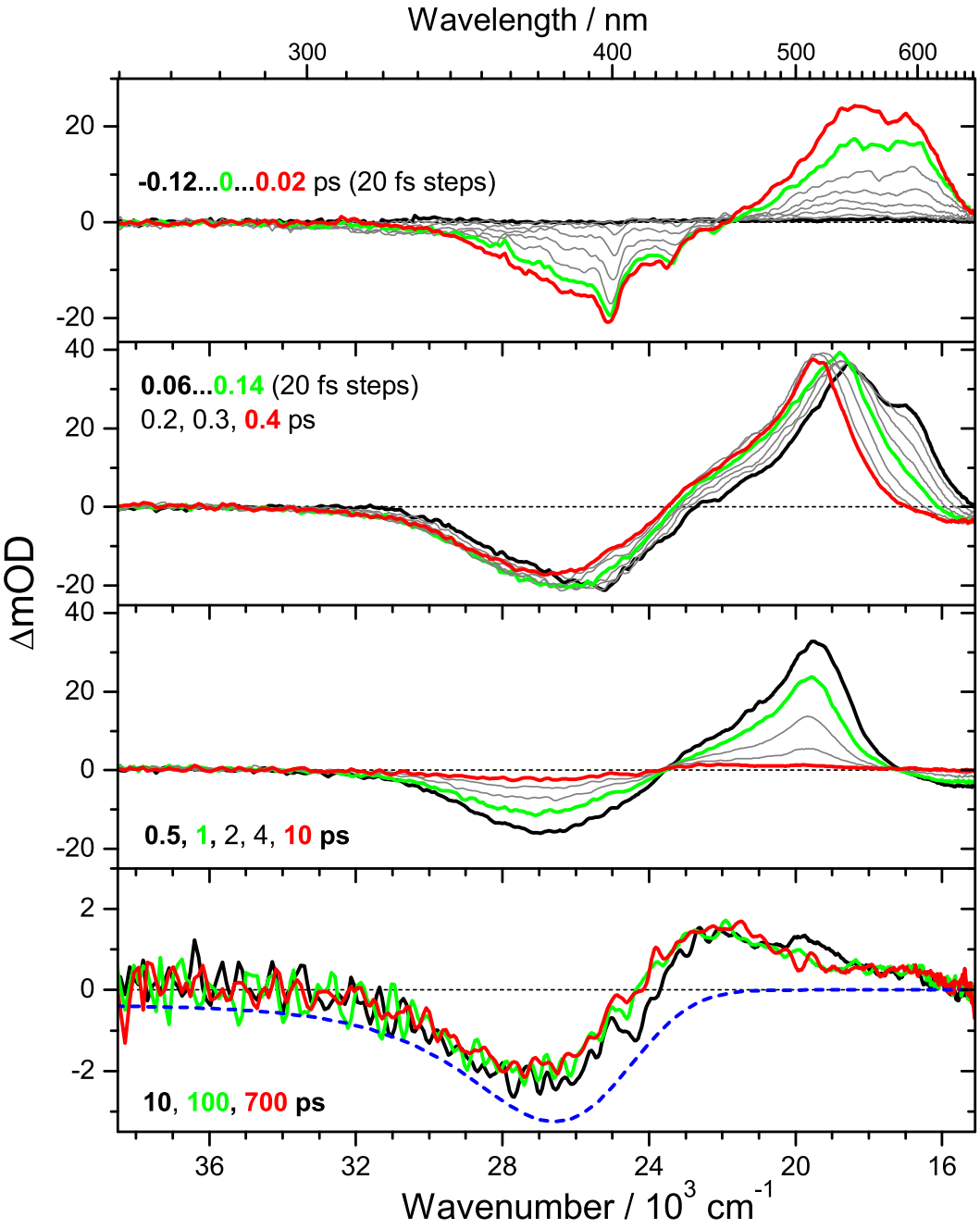

Fig. S19 PSCP transient absorption spectra of all-*trans* retinal in acetonitrile at 298 K. Experimental conditions: λ_{pump} = 400 nm; fluence of the pump pulse *ca.* 0.23 mJ cm^{-2}. In the bottom panel, the inverted steady-state absorption spectrum is shown for comparison.

Overview of time constants and quantum yields from the global analysis

Table S2 Kinetic parameters from the global analysis for all-*trans* retinal, 13-*cis* retinal and all-*trans* retinoic acid upon excitation at 400 nm.

Solvent	Δf [a]	τ_{CC} [b] (fs)	S_2					S_1				ICT			$^1n\pi^*$	Quantum yield (%) [d]		
			$\tau_{2,S1}$ ($S_2\rightarrow S_1$) (ps)	$\tau_{2,ICT}$ ($S_2\rightarrow$ICT) (ps)	τ_2 [c] (ps)	Φ_{S1} (%)	Φ_{ICT} (%)	$\tau_{1,n\pi^*}$ ($S_1\rightarrow{}^1n\pi^*$) (ps)	$\tau_{1,trans}$ ($S_1\rightarrow S_{0,trans}$) (ps)	$\tau_{1,cis}$ ($S_1\rightarrow S_{0,cis}$) (ps)	τ_1 [c] (ps)	$\tau_{ICT,trans}$ (ICT$\rightarrow S_{0,trans}$) (ps)	$\tau_{ICT,cis}$ (ICT$\rightarrow S_{0,cis}$) (ps)	τ_{ICT} [c] (ps)	$\tau_{n\pi^*}$ ($^1n\pi^*\rightarrow T_1$) (ps)	Φ_{T1} (= $\Phi_{n\pi^*}$)	Φ_{trans}	Φ_{cis}
all-*trans* Retinal																		
n-Hexane	0	71	0.075	0.201	0.055	73	27	0.21	2.8	3.5	0.19	1.3	3.0	0.90	31.3	64	24	12
n-Hexadecane	0	63	0.079	0.246	0.060	76	24	0.21	2.9	3.5	0.19	1.0	3.0	0.74	31.7	67	23	10
Diisopropyl ether	0.28	57	0.127	0.355	0.094	74	26	0.26	2.0	5.0	0.22	2.8	6.0	1.9	30.8	62	26	12
THF	0.44	82	0.150	0.158	0.077	51	49	0.56	0.88	5.1	0.32	3.4	6.4	2.2	20	29	51	20
Ethanol	0.67	92	0.113	0.099	0.053	47	53	2.7	0.78	1.8	0.45	2.0	9.0	1.6	22	8	71	21
Methanol	0.71	82	0.113	0.093	0.051	45	55	4.7	0.49	3.8	0.39	1.9	12	1.7	27	4	84	12
Acetonitrile	0.71	80	0.154	0.115	0.066	43	57	3.0	0.42	1.7	0.30	2.2	20	1.9	20	4	83	13
13-*cis* Retinal																		
n-Hexane	0	60	0.065	0.141	0.045	68	32	0.15	1.0	0.61	0.11	3.1	0.84	0.67	27.2	49	14	37
Acetonitrile	0.71	77	0.156	0.134	0.072	46	54	0.89	2.0	0.12	0.10	20	1.3	1.3	20	5	6	89

			S_2	S_1/ICT			Quantum yield (%)	
			τ_2($S_2\rightarrow S_1$/ICT) (ps)	$\tau_{1,trans}$(S_1/ICT$\rightarrow S_{0,trans}$) (ps)	$\tau_{1,cis}$(S_1/ICT$\rightarrow S_{0,cis}$) (ps)	$\tau_{S1/ICT}$ [c] (ps)	Φ_{trans}	Φ_{cis}
all-*trans* Retinoic acid								
n-Hexane	0	81	0.127	20.1	550	19.4	97	3

[a] Dipolarity $\Delta f = R(\varepsilon)\text{-}R(n) = (\varepsilon\text{-}1)/(\varepsilon\text{+}2)\text{-}(n\text{-}1)/(n\text{+}2)$ where ε and n are the dielectric constant and the refractive index of the solvent, respectively.

[b] Pump-probe intensity cross-correlation of the experiment.

[c] τ_2, τ_1 and τ_{ICT} represent the total lifetime of the S_2, S_1 and ICT species, respectively. For all-*trans* retinoic acid in *n*-hexane, there is no experimental indication for separate S_1 and ICT species. Therefore we assume a single S_1/ICT state with the total lifetime $\tau_{S1/ICT}$.

[d] The quantum yield Φ_{trans} corresponds to formation of the *trans* isomer from the S_1 and ICT channels. According to Yuzawa *et al.*,[9] all-*trans* retinal does not isomerise in the triplet channel, so in that case $\Phi_{trans}(\text{total}) \approx \Phi_{trans} + \Phi_{T_1}$. For 13-*cis* retinal, our $T_1\rightarrow T_n$ spectra suggest that 13-*cis* is the dominant species in the triplet channel, therefore here $\Phi_{13\text{-}cis}(\text{total}) \approx \Phi_{13\text{-}cis} + \Phi_{T_1}$. Obviously, there is a high propensity to form the isomer which was originally photoexcited.

Species-associated spectra for all-*trans* retinal in different solvents

Species-associated spectra (SAS) for all-*trans* retinal in the solvents *n*-hexadecane, diisopropyl ether, THF and acetonitrile obtained from global kinetic analysis according to the model in Fig. 4(A) (main manuscript) are shown in Fig. S20. For diisopropyl ether (B), the absorption below 31000 cm^{-1} in the S_2 spectrum arises from residual coherent solvent signal contributions during the pump-probe overlap time which cannot be corrected by subtraction.

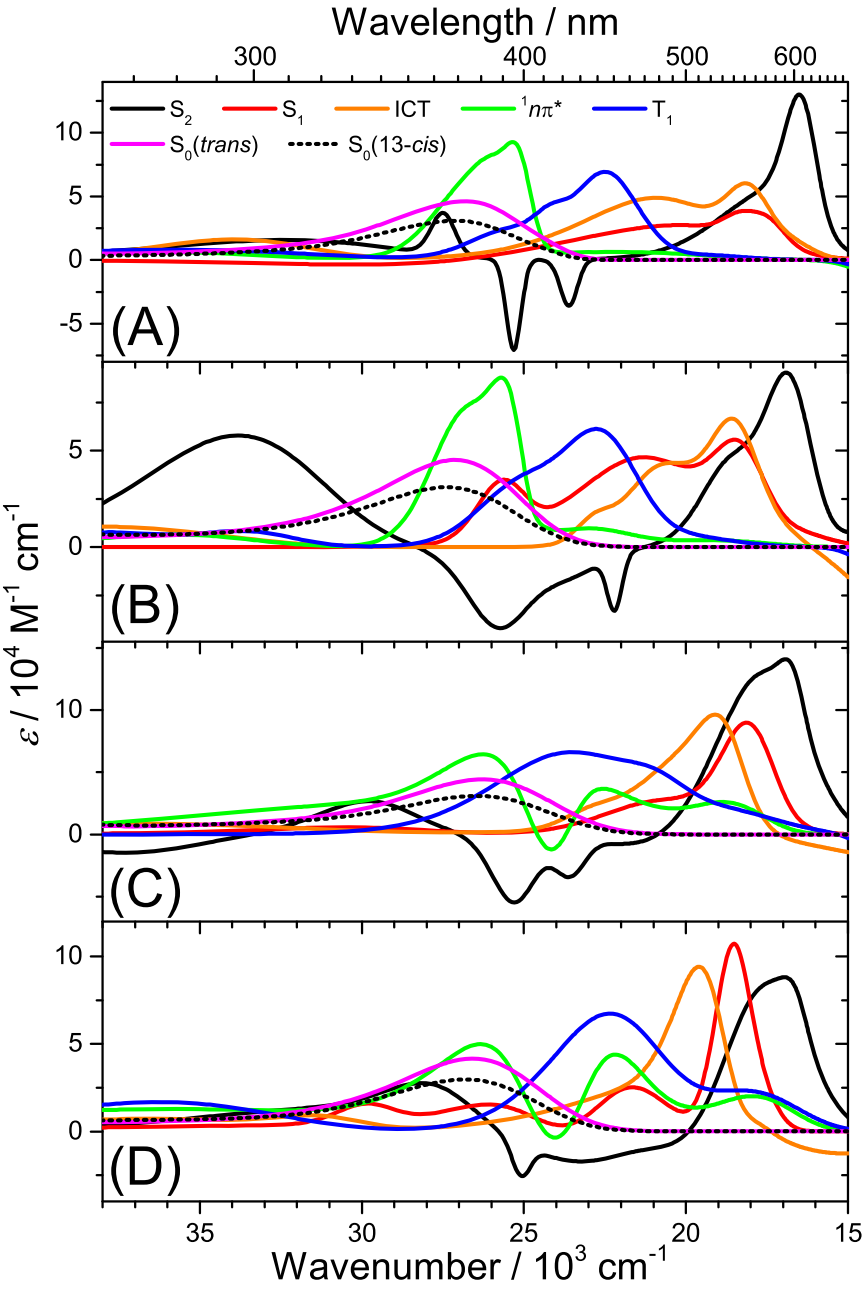

Fig. S20 Comparison of SAS from the global kinetic analysis of UV-Vis PSCP transient absorption spectra for all-*trans* retinal in (A) *n*-hexadecane, (B) diisopropyl ether, (C) THF, and (D) acetonitrile. The different colours indicate the different species which were included in the global kinetic modelling: S_2 (black), S_1 (red), ICT (orange), $^1n\pi^*$ (green), T_1 (blue), S_0 of all-*trans* retinal (magenta) and S_0 of 13-*cis* retinal (black-dotted line).

Spectral fits and kinetics for all-*trans* retinal in different solvents

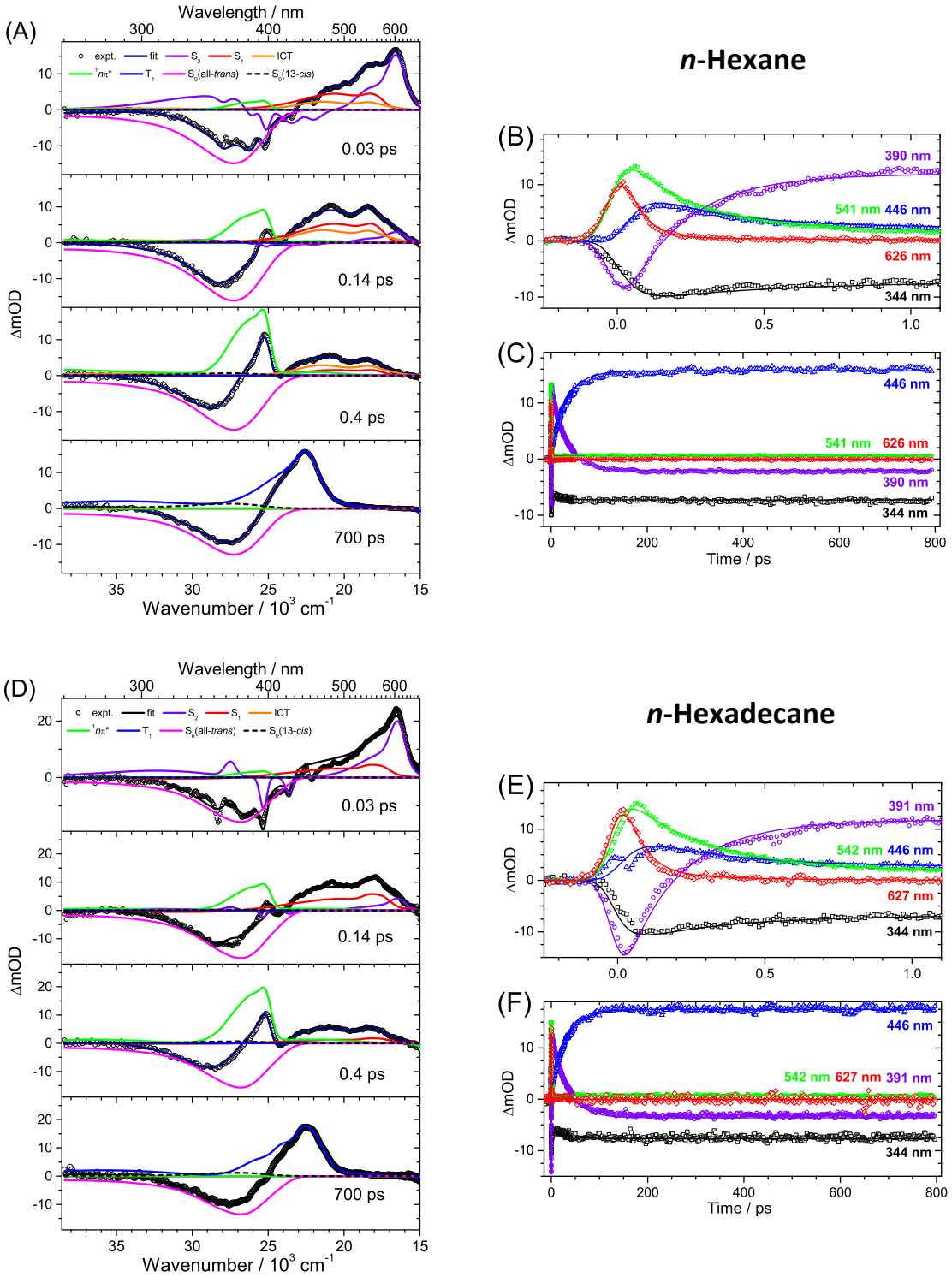

Fig. S21 Contributions of the different transient species to the experimental PSCP spectra and kinetics of all-*trans* retinal in *n*-hexane (A-C) and *n*-hexadecane (D-F). Spectra are shown at four selected times, and kinetic traces are compared at five different wavelengths on short and long time scales including fit lines.

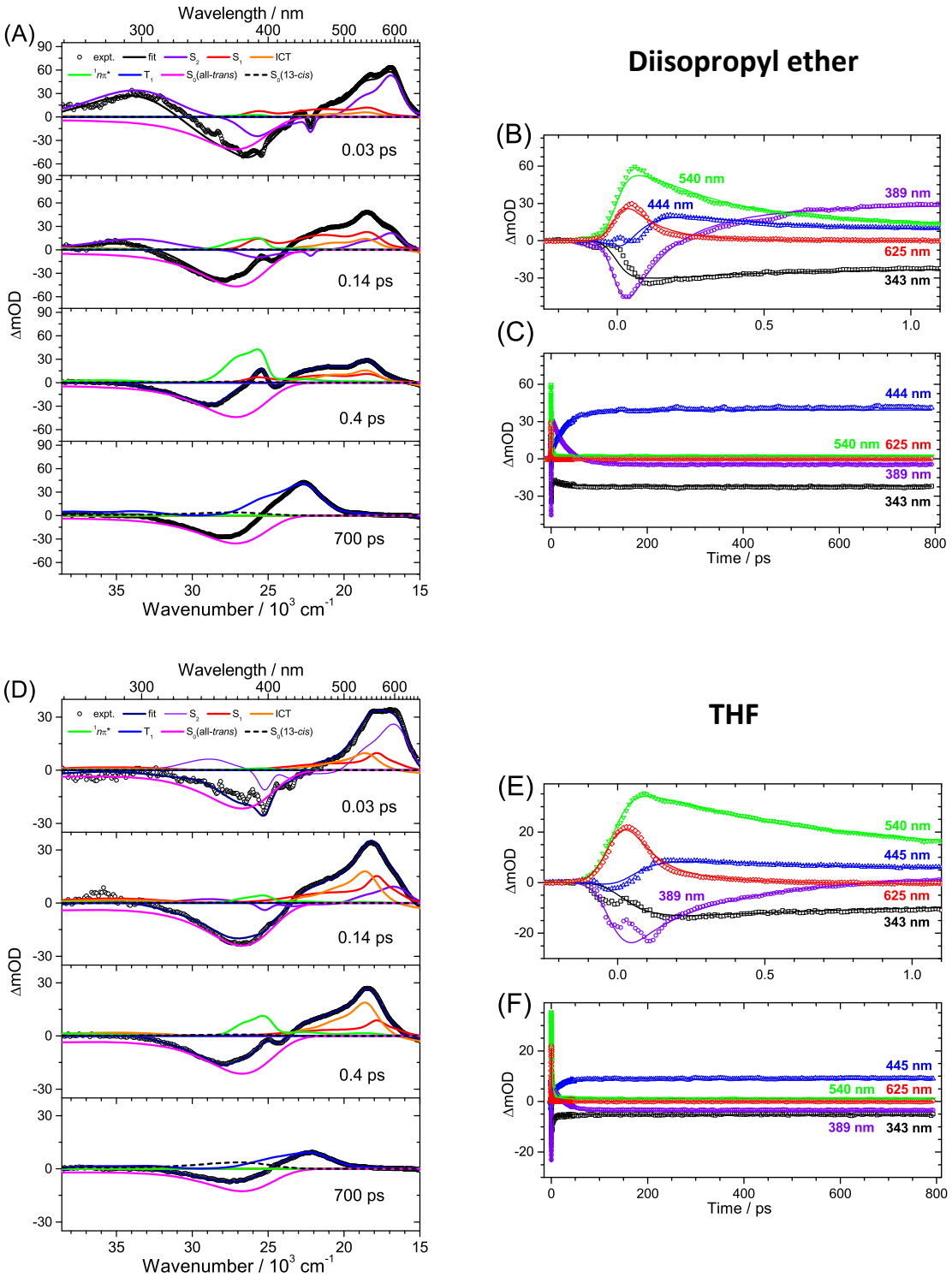

Fig. S22 Contributions of the different transient species to the experimental PSCP spectra and kinetics of all-*trans* retinal in diisopropyl ether (A-C) and THF (D-F). Spectra are shown at four selected times, and kinetic traces are compared at five different wavelengths on short and long time scales including fit lines.

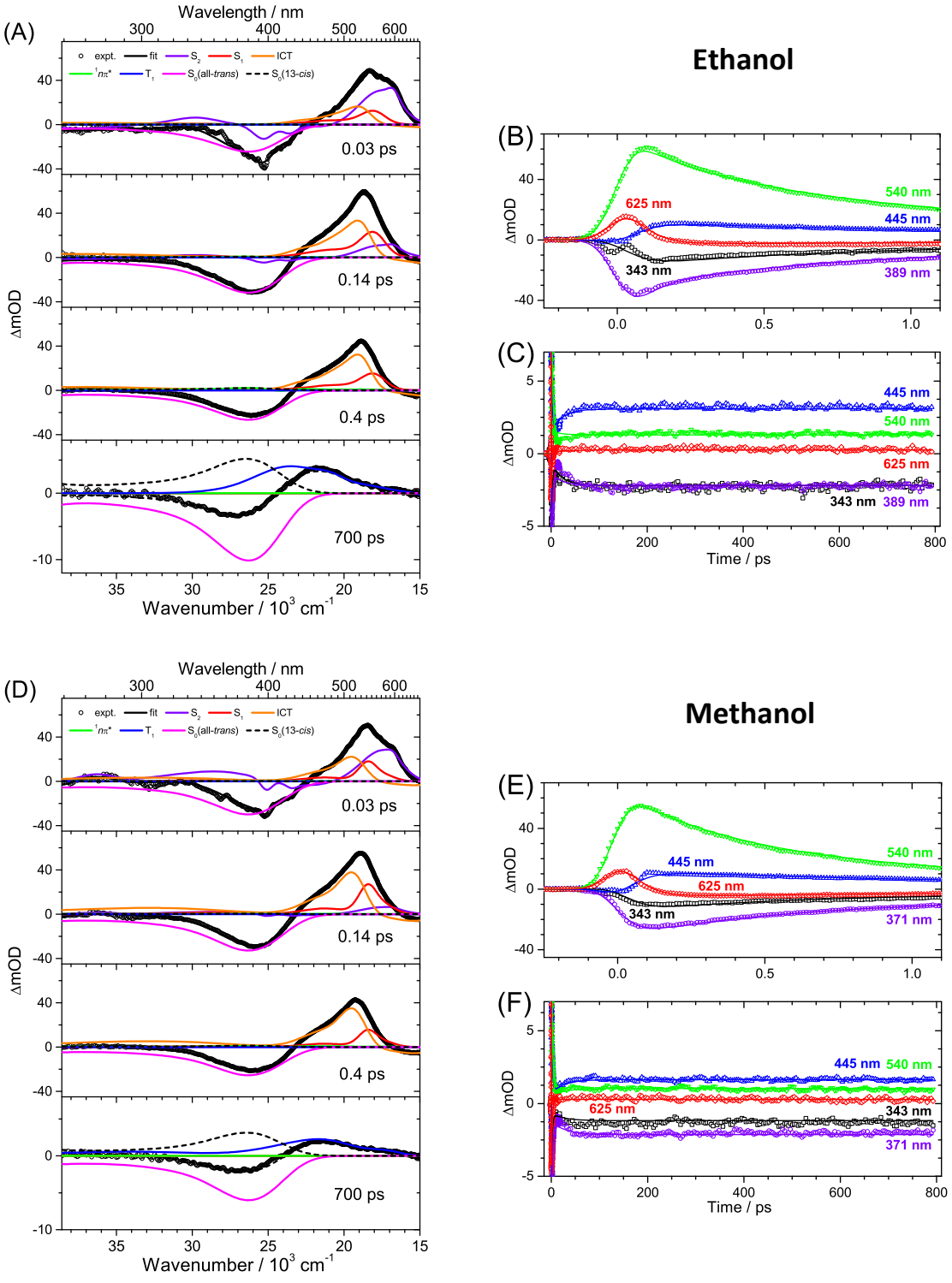

Fig. S23 Contributions of the different transient species to the experimental PSCP spectra and kinetics of all-*trans* retinal in ethanol (A-C) and methanol (D-F). Spectra are shown at four selected times, and kinetic traces are compared at five different wavelengths on short and long time scales including fit lines.

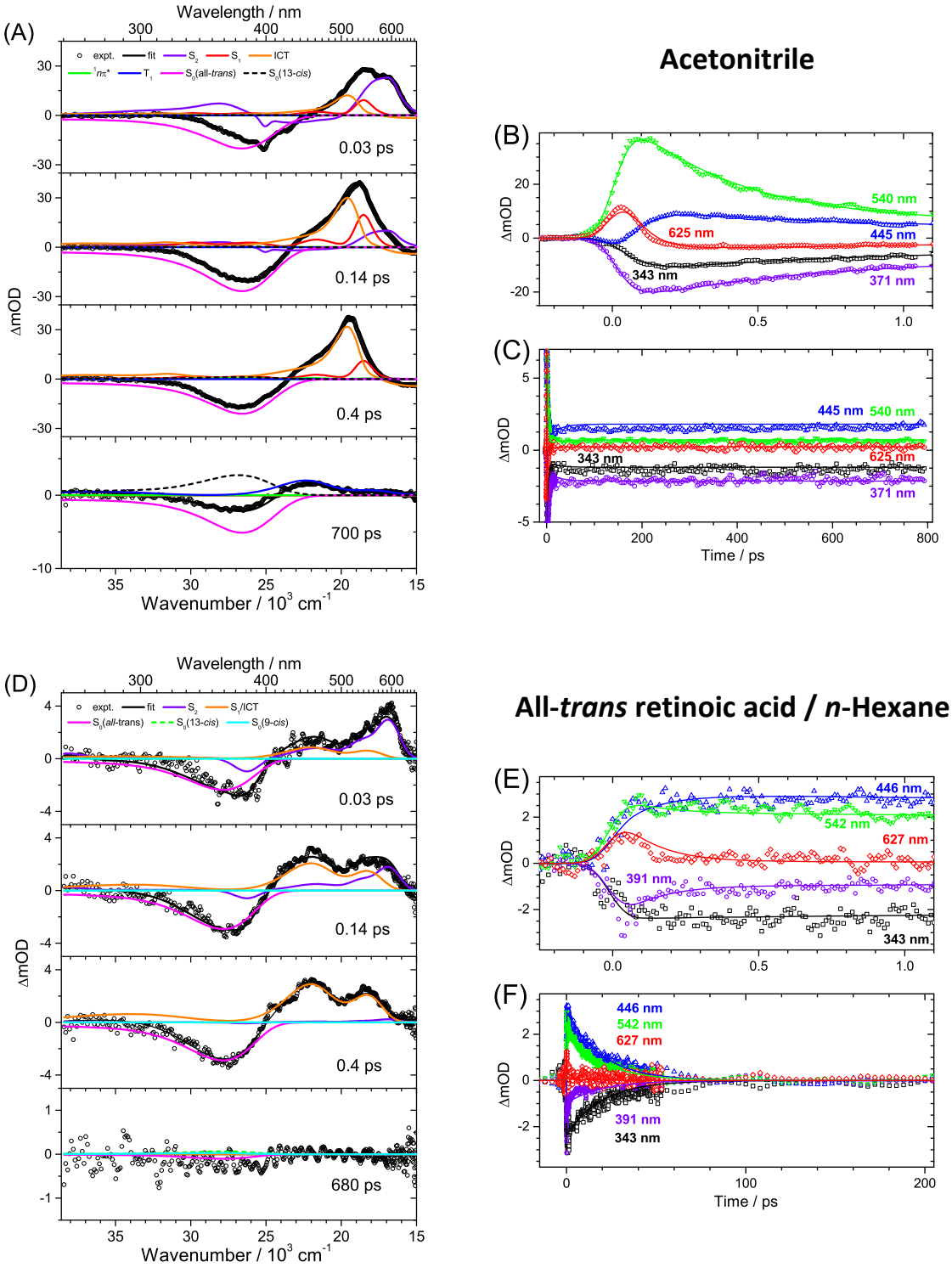

Fig. S24 Contributions of the different transient species to the experimental PSCP spectra and kinetics of all-*trans* retinal in acetonitrile (A-C) and all-*trans* retinoic acid in *n*-hexane (D-F). Spectra are shown at four selected times, and kinetic traces are compared at five different wavelengths on short and long time scales including fit lines.

Comparison with fit results from other kinetic models

Figure S25(A) contains simulations of the experimental kinetic trace at 393 nm for all-*trans* retinal in *n*-hexane using the best model featuring formation of $^1n\pi^*$ from S_1 (Fig. 4(A) in the main manuscript). Figure S25(B) shows results of a model employing initial branching of S_2 into $^1n\pi^*$, S_1 and ICT. The best model in (A) successfully describes the delayed rise of the $^1n\pi^*$ signal (green and black lines). In contrast, the model employing triple branching from S_2 fails, see (B). In the latter case, the $^1n\pi^*$ band rises too quickly, because the fast decay of the S_2 ESA band above 600 nm needs to be fitted simultaneously. The rise of the kinetic simulations in the $^1n\pi^*$ region obtained from the latter model is therefore consistently too steep. An analogous behavior is observed for other solvents.

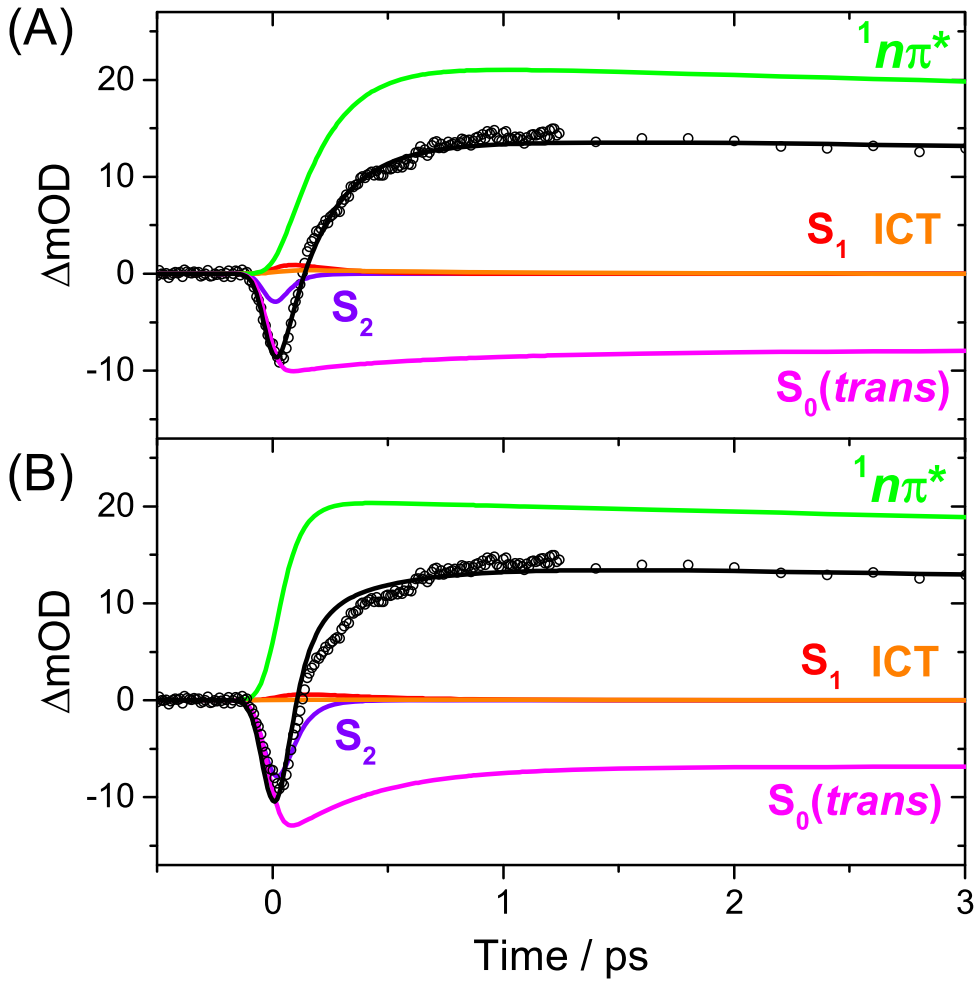

Fig. S25 Simulation of the kinetic trace at 393 nm for all-*trans* retinal in *n*-hexane based on global analysis using the best kinetic model (A) and a model featuring initial branching from S_2 into $^1n\pi^*$, S_1 and ICT (B). The experimental PSCP data are shown as black open circles.

Figure S26(A) shows simulations of the experimental kinetic trace at 531 nm for all-*trans* retinal in THF using the best model employing separate S_1 and ICT species (Fig. 4(A) in the main manuscript). Figure S26(B) shows results of a model featuring a single S_1/ICT state instead. The best model in (A) successfully describes the decay of the ESA band which is not a single exponential. The fast component is due to S_1 (red line), whereas the slower part is due to the ICT species (orange line). In contrast, model (B) using a single S_1/ICT state fails. In the latter case, the S_1/ICT species exhibits a single exponential decay which is not able to describe the second slower decay component. Note that an analogous behavior is observed in other solvents.

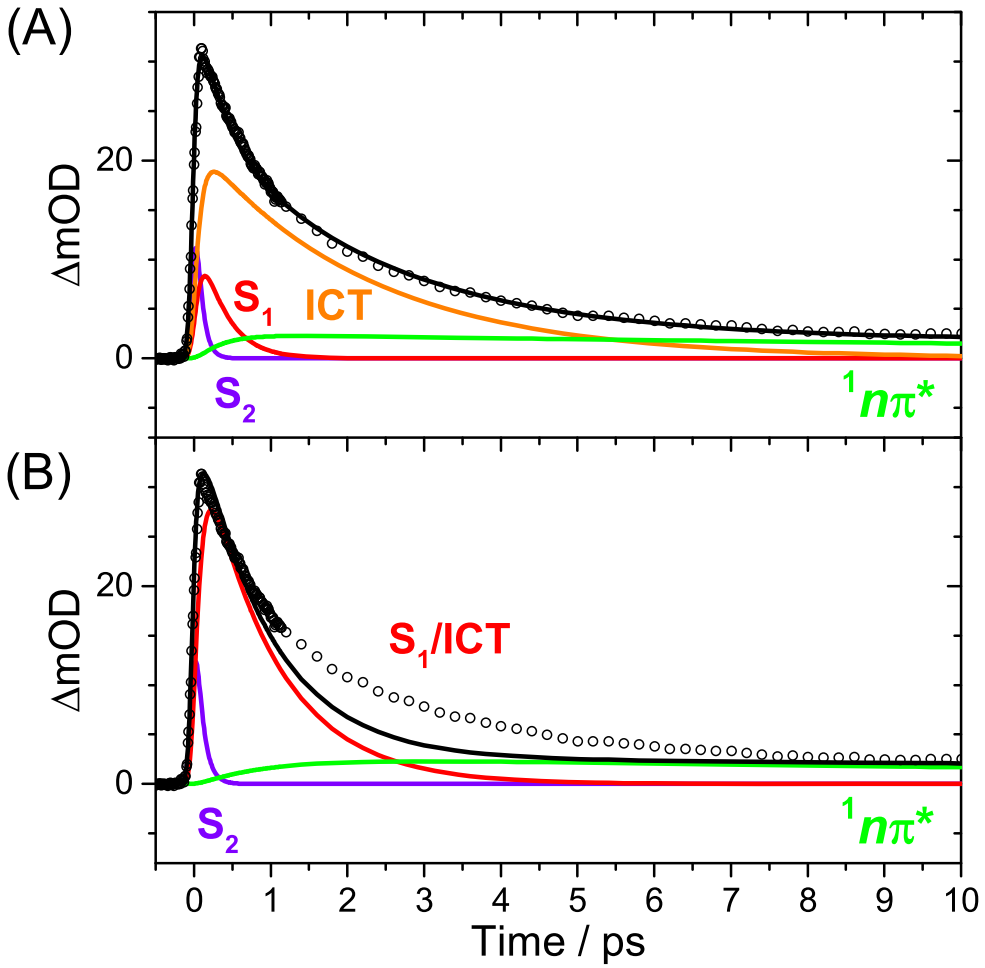

Fig. S26 Comparison of kinetic traces for all-*trans* retinal in THF from the global analysis using the best kinetic model (Fig. 4(A), main manuscript) and a model featuring a single S_1/ICT state. Note that the decay kinetics at 531 nm obtained from the latter model are monoexponential and decay way too fast (B). An adequate modelling of the biexponential decay requires two species (S_1 and ICT) which decay independently (A).

Steady-state absorption spectra for isomers of retinoic acid

In Fig. S27, we provide steady-state absorption spectra of all-*trans*, 13-*cis* and 9-*cis* retinoic acid in *n*-hexane. They were recorded at low concentration (3×10^{-5} M) to minimise the influence of dimer formation. The peak absorption coefficients of the 13-*cis* and 9-*cis* isomers are lower than for the all-*trans* isomer. In addition, the 9-*cis* spectrum is blue-shifted. Therefore, in the case of the transient absorption experiments starting from pure all-*trans* retinoic acid in *n*-hexane, any formation of 13-*cis* and 9-*cis* isomers arising from photoisomerisation must result in a persistent bleach feature at *ca.* 360 nm at long times. This is indeed observed in the PSCP transient absorption spectra (see Fig. 1(B) in the main manuscript, inset in the bottom panel).

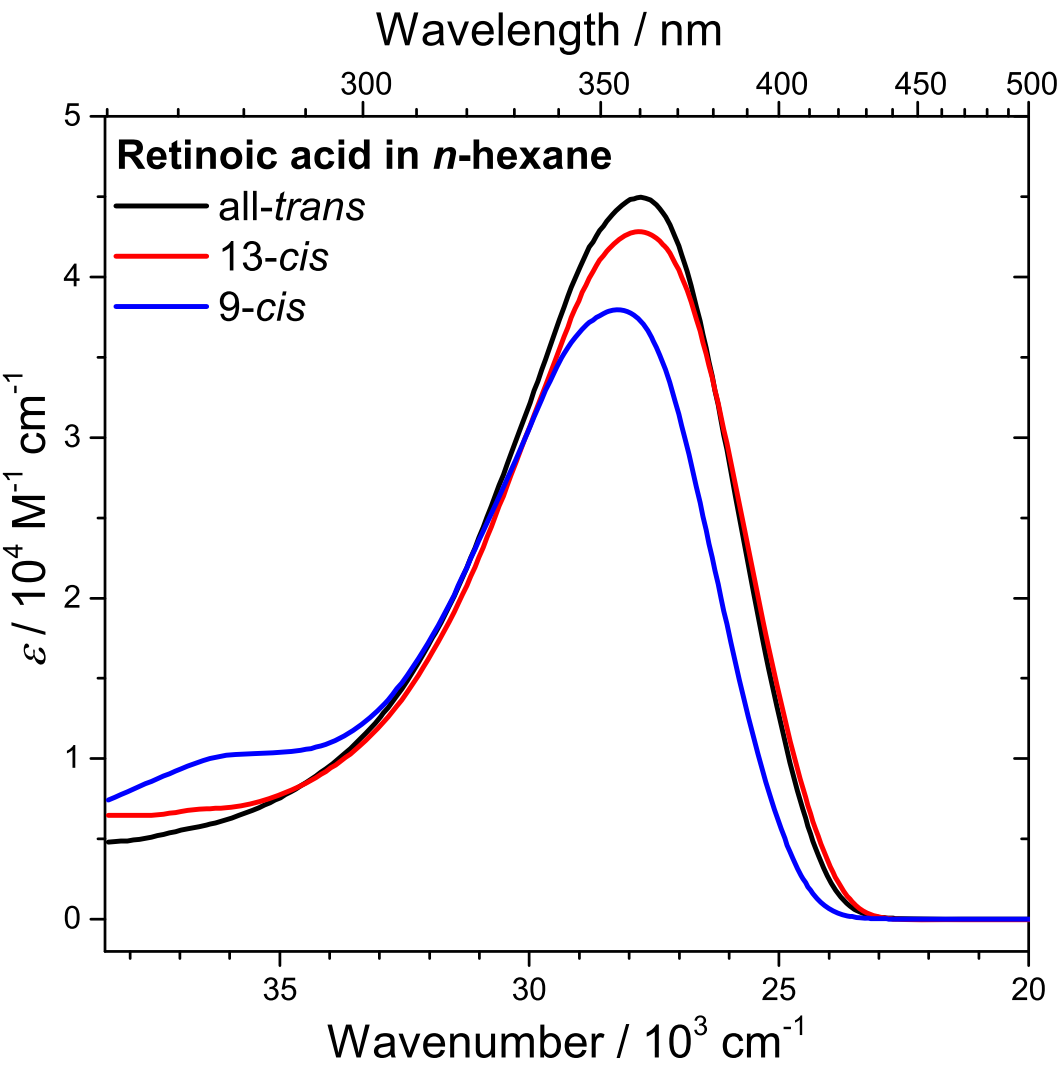

Fig. S27 Steady-state absorption spectra of different retinoic acid isomers in *n*-hexane at room temperature. All-*trans* (black), 13-*cis* (red) and 9-*cis* (blue).

UV-Vis broadband transient absorption spectra of 13-*cis* retinal

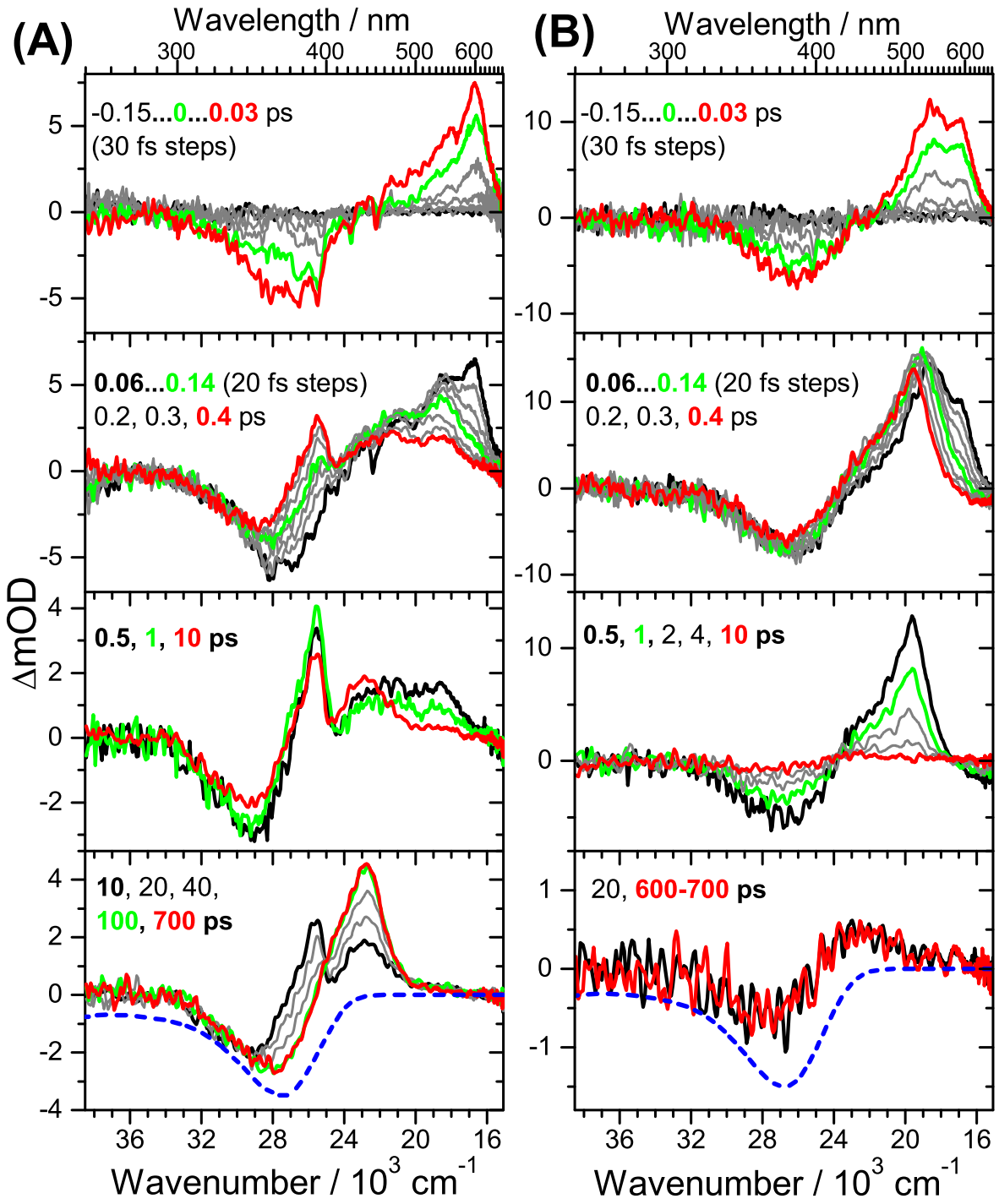

Fig. S28 PSCP spectra of 13-*cis* retinal in (A) *n*-hexane and (B) acetonitrile at 298 K. Experimental conditions: λ_{pump} = 400 nm; fluence of the pump pulse *ca.* 0.23 mJ cm^{-2}. In the bottom panel, the inverted steady-state absorption spectra are shown for comparison as blue-dashed lines. We note that the signal-to-noise ratio in these experiments is reduced due to the lower solubility of the 13-*cis* isomer in organic solvents.

Figure S29 shows normalised PSCP transient absorption spectra at long times as well as the corresponding SAS of the triplet state for all-*trans* retinal and 13-*cis* retinal in *n*-hexane. In the case of the 13-*cis* species, the whole transient spectrum and the triplet SAS are blue-shifted, suggesting that the quantum yield for isomerisation from the 13-*cis* to the all-*trans* form must be small. Otherwise its peak should be located close to the all-*trans* spectrum. This is indeed confirmed by the global kinetic analysis (Table S2, ESI).

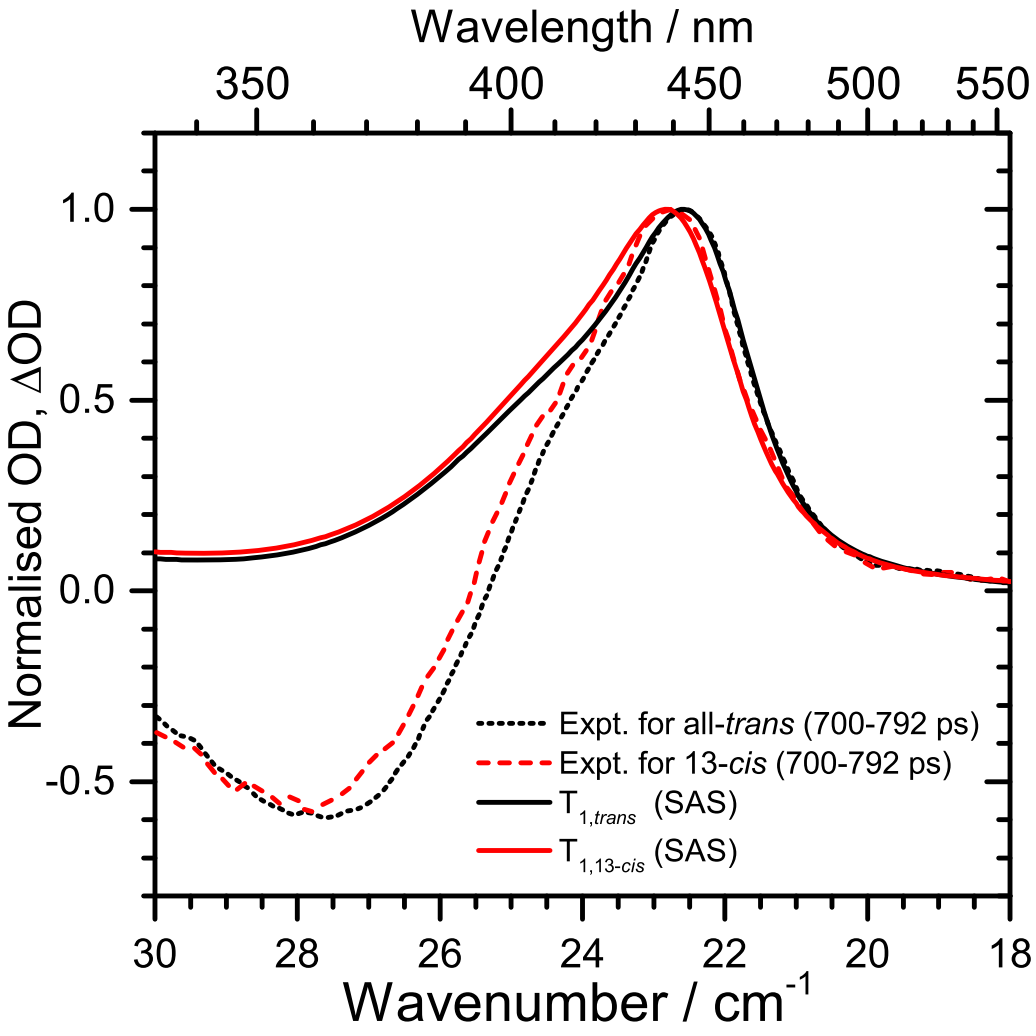

Fig. S29 Comparison of normalised UV-Vis broadband transient absorption spectra at long times and triplet SAS for all-*trans* and 13-*cis* retinal in *n*-hexane. The experimental transient spectra were averaged over the time range 700-792 ps and show GSB and T_1 absorption (black-dotted and red-dashed lines for all-*trans* and 13-*cis*, respectively). The transient spectra are compared with the SAS of the triplet species $T_{1,trans}$ and $T_{1,13\text{-}cis}$ (black and red solid lines, respectively), as obtained from the global kinetic analysis.

Results of DFT/TDDFT calculations for all-*trans* retinal and all-*trans* retinoic acid

The results of the DFT/TDDFT calculations are summarised in Table S3. Transition energies are compared in Figs. S30. Figure S31 contains detachment/attachment electron densities[10] for the three lowest excited electronic states. The optimized ground state structure features an *s-cis* configuration with a torsional angle of 46.9° (all-*trans* retinal) and 47.3° (all-*trans* retinoic acid), in good agreement with our previous results for β-carotene derivatives.[11] We note that the Tamm-Dancoff approximation (TDA) barely affects the position of the $S_0 \rightarrow {}^1n\pi^*$ transition (59-197 cm^{-1} for all-*trans* retinal and 6-125 cm^{-1} for all-*trans* retinoic acid, depending on the functional), whereas the transitions of the other two singlet states shift more: In the case of the lower state one obtains 902-1727 cm^{-1} for all-*trans* retinal and 935-1730 cm^{-1} for all-*trans* retinoic acid, respectively. In contrast, for the higher state one finds 1287-1981 cm^{-1} for all-*trans* retinal and 1292-2070 cm^{-1} for all-*trans* retinoic acid, respectively. In some cases, this effect changes the state ordering, making the optically dark ${}^1n\pi^*$ state the lowest excited singlet state for all-*trans* retinal (B3LYP and CAM-B3LYP) or the second lowest excited singlet state for all-*trans* retinoic acid (CAM-B3LYP).

Table S3 Gas-phase transition wavenumber $\tilde{\nu}$ and oscillator strength *f* from DFT/TDDFT calculations for the three energetically lowest excited singlet states (numbered according to energy) of all-*trans* retinal and all-*trans* retinoic acid using the functionals SVWN, BLYP, B3LYP, MPW1K and CAM-B3LYP. Results in parentheses are obtained using the Tamm-Dancoff approximation (TDA).

State	SVWN		BLYP		B3LYP		MPW1K		CAM-B3LYP	
	$\tilde{\nu}$ / cm^{-1}	*f*	$\tilde{\nu}$ / cm^{-1}	*f*	$\tilde{\nu}$ / cm^{-1}	*f*	$\tilde{\nu}$ / cm^{-1}	*f*	$\tilde{\nu}$ / cm^{-1}	*f*
all-*trans* Retinal										
S_1	18005 (18092)	0.00 (0.00)	19236 (19295)	0.00 (0.00)	23953 (25326)	1.24 (0.00)	27007 (---)	1.68 (---)	27486 (29000)	1.72 (0.00)
S_2	19966 (20868)	0.63 (0.59)	20320 (21261)	0.67 (0.63)	25208 (25397)	0.00 (1.35)	29204 (---)	0.00 (---)	28803 (29213)	0.00 (2.15)
S_3	26248 (28229)	0.95 (0.87)	26445 (28438)	0.93 (0.96)	30771 (32248)	0.56 (1.28)	36246 (---)	0.28 (---)	37524 (38811)	0.20 (0.40)
all-*trans* Retinoic acid										
S_1	20743 (21678)	0.68 (0.64)	21064 (22044)	0.74 (0.68)	24568 (26042)	1.29 (1.43)	27542 (---)	1.68 (---)	27967 (29697)	1.70 (2.12)
S_2	25841 (25847)	0.00 (0.00)	26270 (26286)	0.00 (0.00)	31400 (32748)	0.52 (1.18)	36808 (---)	0.25 (---)	38019 (38423)	0.18 (0.00)
S_3	26841 (28911)	0.94 (1.26)	27003 (29059)	0.91 (1.42)	33333 (33391)	0.00 (0.00)	39067 (---)	0.00 (---)	38298 (39311)	0.00 (0.35)

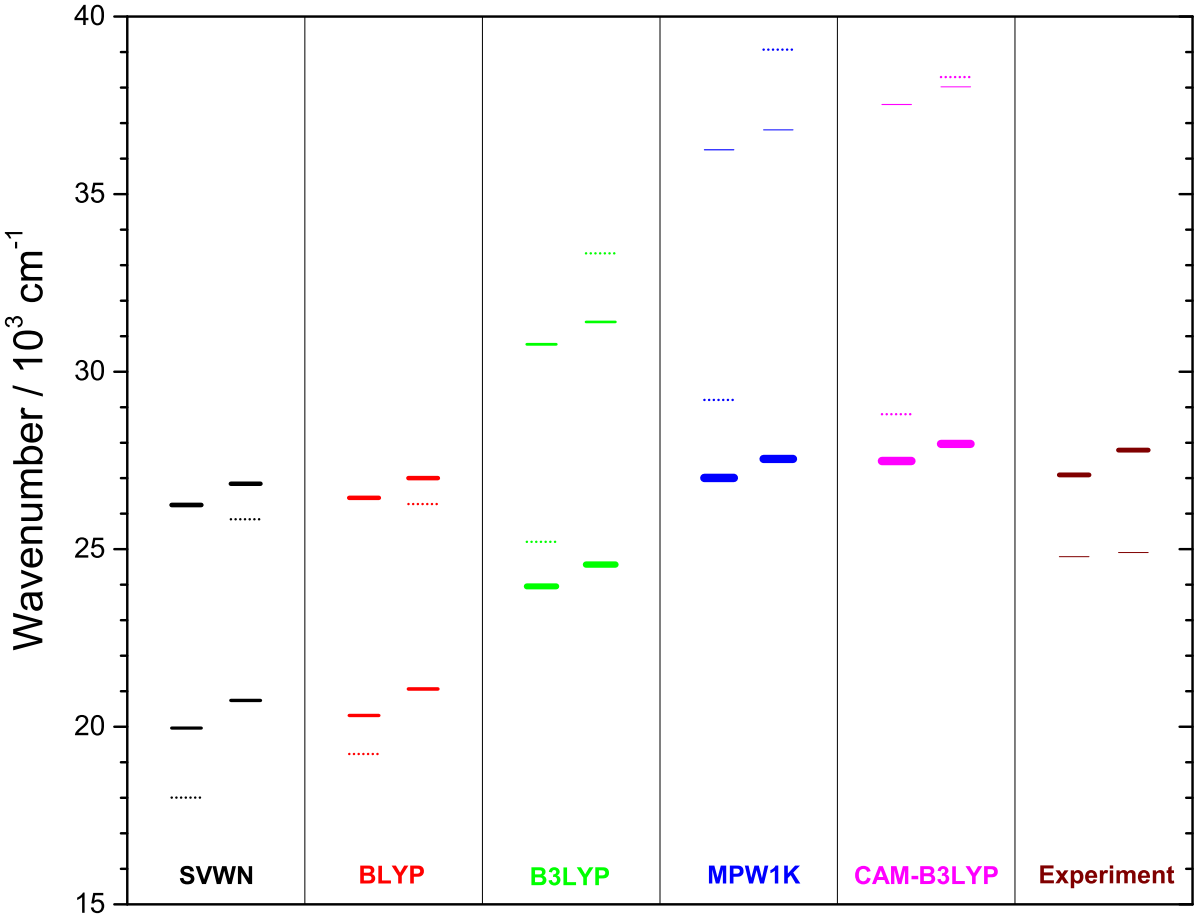

Fig. S30 Level diagram for the three energetically lowest singlet state transitions from gas-phase DFT/TDDFT calculations according to Table S3 (without TDA). The functionals SVWN, BLYP, B3LYP, MPW1K and CAM-B3LYP were used. For each functional, the levels on the left are for all-*trans* retinal, whereas the levels on the right are for all-*trans* retinoic acid. In each case, the dotted line denotes the $S_0 \rightarrow {}^1n\pi^*$ transition (zero oscillator strength) whereas the solid lines are for the $S_0 \rightarrow {}^1A_g^-$ and $S_0 \rightarrow {}^1B_u^+$ transitions. For the latter two, the thickness of each solid line is proportional to the calculated oscillator strength. In the rightmost column, the experimental values for the $S_0 \rightarrow {}^1B_u^+$ transition (thick lines) are determined from the maximum of the respective steady-state absorption spectrum in *n*-hexane. According to Birge *et al.*,[12] the $S_0 \rightarrow {}^1A_g^-$ transition (thin line) of all-*trans* retinal is estimated to lie 2300 cm^{-1} below $S_0 \rightarrow {}^1B_u^+$. In the case of all-*trans* retinoic acid, Koyama and co-workers estimate a value of 2900 cm^{-1} for this spacing.[13] An experimental determination of the optically dark $S_0 \rightarrow {}^1n\pi^*$ transition is difficult, but our transient absorption experiments suggest that it is located below $S_0 \rightarrow {}^1A_g^-$ for all-*trans* retinal and above $S_0 \rightarrow {}^1A_g^-$ for all-*trans* retinoic acid.

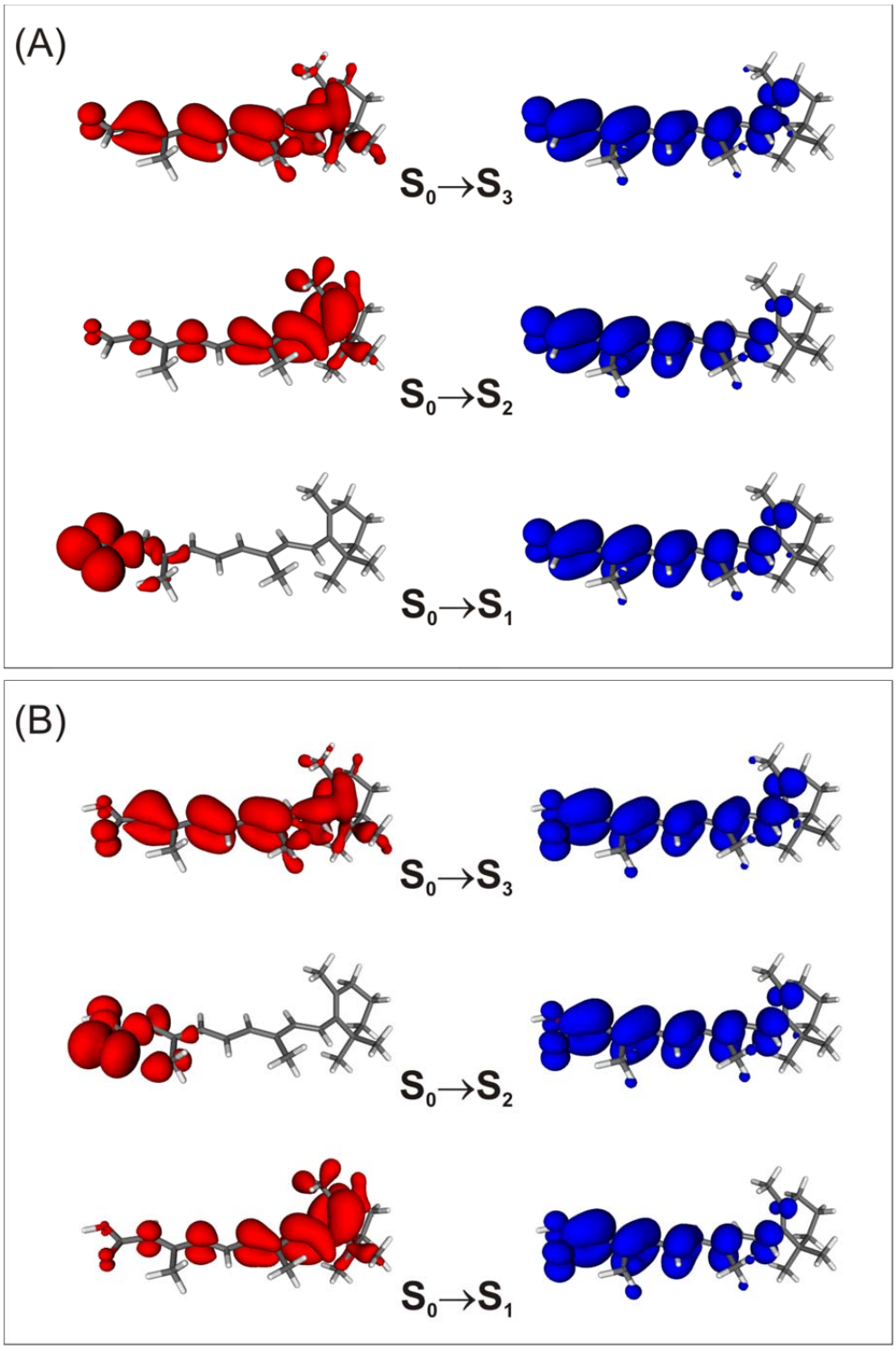

Fig. S31 Detachment (red) and attachment (blue) electron densities for all-*trans* retinal (A) and all-*trans* retinoic acid (B). In each case, the $S_0 \rightarrow S_1$ (bottom), $S_0 \rightarrow S_2$ (middle) and $S_0 \rightarrow S_3$ (top) transitions are shown. The BLYP functional was employed.

References

1. P. W. Lohse, F. Ehlers, K. Oum, M. Scholz and T. Lenzer, *Chem. Phys.*, 2010, **373**, 45.
2. K. Bobrowski and P. K. Das, *J. Phys. Chem.*, 1986, **90**, 927.
3. S. A. Kovalenko, A. L. Dobryakov, J. Ruthmann and N. P. Ernsting, *Phys. Rev. A*, 1999, **59**, 2369.
4. M. Kopczynski, F. Ehlers, T. Lenzer and K. Oum, *J. Phys. Chem. A*, 2007, **111**, 5370.
5. D. A. Wild, K. Winkler, S. Stalke, K. Oum and T. Lenzer, *Phys. Chem. Chem. Phys.*, 2006, **8**, 2499.
6. R. Hemley and B. E. Kohler, *Biophys. J.*, 1977, **20**, 377.
7. R. L. Christensen, M. Goyette, L. Gallagher, J. Duncan, B. DeCoster, J. Lugtenburg, F. J. Jansen and I. van der Hoef, *J. Phys. Chem. A*, 1999, **103**, 2399.
8. P. W. Lohse, R. Bürsing, T. Lenzer and K. Oum, *J. Phys. Chem. B*, 2008, **112**, 3048.
9. T. Yuzawa and H. Hamaguchi, *J. Mol. Struct.*, 1995, **352/353**, 489.
10. S. Hirata and M. Head-Gordon, *Chem. Phys. Lett.*, 1999, **314**, 291.
11. K. Golibrzuch, F. Ehlers, M. Scholz, R. Oswald, T. Lenzer, K. Oum, H. Kim and S. Koo, *Phys. Chem. Chem. Phys.*, 2011, **13**, 6340.
12. R. R. Birge, J. A. Bennett, L. M. Hubbard, H. L. Fang, B. M. Pierce, D. S. Kliger and G. E. Leroi, *J. Am. Chem. Soc.*, 1982, **104**, 2919.
13. J. Xiang, F. S. Rondonuwu, Y. Kakitani, R. Fujii, Y. Watanabe, Y. Koyama, H. Nagae, Y. Yamano and M. Ito, *J. Phys. Chem. B*, 2005, **109**, 17066.